Editors' Suggestion

Fission-fragment yields and prompt-neutron multiplicity for Coulomb-induced fission of ^{234,235}U and ^{237,238}Np

J.-F. Martin,[1] J. Taïeb,[1,2] G. Boutoux,[1] A. Chatillon [ORCID],[1,2,*] T. Gorbinet,[1] E. Pellereau,[1] L. Audouin,[3] A. Heinz,[4]
H. Alvarez-Pol,[5] Y. Ayyad,[5] G. Bélier,[1,2] J. Benlliure,[5] M. Caamaño,[5] E. Casarejos,[6] D. Cortina-Gil,[5] A. Ebran,[1,2] F. Farget,[7]
B. Fernández-Domínguez,[5] L. Grente,[1] H. T. Johansson,[4] B. Jurado,[8] A. Kelić-Heil,[9] N. Kurz,[9] B. Laurent,[1,2] C. Nociforo,[9]
C. Paradela,[5,†] S. Pietri,[9] A. Prochazka,[9] J. L. Rodríguez-Sánchez,[5,‡] D. Rossi,[9,§] H. Simon,[9]
L. Tassan-Got,[3] J. Vargas,[5,‖] B. Voss,[9] and H. Weick[9]

[1]*CEA, DAM, DIF, F-91297 Arpajon, France*
[2]*Université Paris-Saclay, CEA, Laboratoire Matière en Conditions Extrêmes, F-91680 Bruyères-le-Châtel, France*
[3]*Université Paris-Saclay, CNRS/IN2P3, IJCLab, 91405 Orsay, France*
[4]*Department of Physics, Chalmers University of Technology, 412 96 Göteborg, Sweden*
[5]*IGFAE, Instituto Galego de Física de Altas Enerxías, Universidade de Santiago de Compostela, E-15782 Santiago de Compostela, Spain*
[6]*CINTECX, Universidade de Vigo, E-36310 Vigo, Spain*
[7]*CNRS/IN2P3, LPC-Caen, 14000 Caen, France*
[8]*CNRS, CENBG, F-33175 Gradignan, France*
[9]*GSI-Helmholtzzentrum für Schwerionenforschung GmbH, D-64291 Darmstadt, Germany*

Low-energy fission of ^{234,235}U and ^{237,238}Np radioactive beams, provided by the Fragment Separator (FRS) of the GSI Helmholtzzentrum für Schwerionenforschung facility (GSI), has been studied using the Reactions with Relativistic Radioactive Beams / Studies on Fission with Aladin (R3B/SOFIA) setup. The latter allows us, on an event-by-event basis, to simultaneously identify, in terms of their mass and atomic numbers, the fissioning nucleus in coincidence with both fission fragments after prompt-neutron emission. This article reports new results on elemental, isotonic, isobaric, and isotopic yields. Moreover, the high accuracy of our data allowed us to study in detail proton even-odd staggering, from elemental yields; neutron excess, from isotopic yields; and total prompt-neutron multiplicity, from the difference of masses of the fissioning nucleus and fission fragments. These results are then compared to previous experimental data in order to probe how these fission observables change as function of the excitation energy and atomic and neutron numbers of the compound nucleus.

I. INTRODUCTION

Fission is one of the most dramatic reactions a nucleus can suffer: It leads to extreme deformations and results in a complete rearrangement of all nucleons. A large variety of observables of the fission process have been probed both through experimental and theoretical approaches. These observables include the fission cross sections, the energy and multiplicity of prompt neutrons and γ radiations, the yields of the fission fragments, and their kinetic energy. Such observables depend on the isotope which undergoes fission and the excitation energy at which fission occurs. The Reactions with Relativistic Radioactive Beams / Studies on Fission with Aladin (R3B/SOFIA) experiment focuses on fission yields, which are of high interest both for application purposes and for a theoretical description of reactions and the connection to nuclear structure.

In the field of nuclear technology, fission yields are mostly important in nuclear power plants. With increasing use of the fissile fuel, the inventory of fission fragments (and subsequent decay products) becomes more important in the reactor core. Under normal running conditions, some fragments show a very high neutron-absorption cross section: They are thus considered as poisons and reduce reactivity. Other fragments emit delayed neutrons, which are essential for the control of the fission rate. In abnormal conditions, the fission chain reaction is stopped, as well as all prompt-energy release. However, the delayed decay of the fission fragments is responsible for the residual power of the core, which amounts to approximately 6% of the nominal value and decreases steadily with time. An accurate estimate of this decay heat is paramount for the design of cooling systems for the reactor to cope with this residual energy and to avoid a meltdown of the core. Such an

*audrey.chatillon@cea.fr

†Present address: EC-JRC, Institute for Reference Materials and Measurements, Retieseweg 111, B-2440 Geel, Belgium.

‡Present address: GSI-Helmholtzzentrum für Schwerionenforschung GmbH, D-64291 Darmstadt, Germany.

§Present address: Technische Universität Darmstadt, Fachbereich Physik, Institut für Kernphysik, Schlossgartenstrasse 9, 64289 Darmstadt, Germany.

‖Present address: Universidad Santo Tomás, Tunja, Colombia.

estimate relies on precise and accurate knowledge of yields, half-lives, and decay energies of the fission fragments.

Fission-fragment yields also probe the influence of nuclear structure of nuclei at extreme deformation on fission, all the more when the yields are correlated with the total neutron multiplicity (ν_{tot}) or the total kinetic energy (TKE). Microscopically, the fission process can be described as the evolution of the compound nucleus along the valleys of the potential energy surface (PES), calculated from the binding energy of the system in a given deformation subspace. An interpretation of the fission observables [1–3] states that each valley results in a different fission mode, each characterized by its own barrier and scission configuration and governed by the shell structure of the nascent fission fragments. In the near-stable actinide region, the focus of this article, a competition between three main fission modes has been proposed. The standard I (ST1) asymmetric mode is governed by the doubly magic shell closure around ^{132}Sn, leading to an almost spherical heavy fragment and therefore a compact scission configuration. The standard II (ST2) asymmetric mode is characterized by a heavy fragment stabilized around $Z = 54$ [4], which has been recently related to a proton shell in the octupole-deformed fragments [5]. Finally, the superlong (SL) symmetric mode leads to two, on average, mass-symmetric fission fragments, which are both highly deformed. This mode prevails at higher excitation energy, as the microscopic shell structure is progressively dampened.

In this article, the experimental setup is briefly presented in Sec. II. Then, all experimental results obtained on the fission yields for the ^{234,235}U fissioning nuclei are detailed in Sec. III. The prompt-neutron multiplicity as a function of the isotopic yields is also studied in Sec. III E to probe the scission configurations. Additional results on the fission yields of neptunium isotopes are presented in Sec. IV. The latter data are used in Sec. V to investigate the discrepancies or similarities between neighboring even-Z and odd-Z fissioning nuclei by measuring how the mean values of the fission yields depend on the number of protons and neutrons of the fissioning compound nuclei. Finally, a comparison is performed in Sec. VII between different models to estimate the number of neutrons of the fission fragments at scission, before the prompt-neutron evaporation phase.

II. R3B/SOFIA experiment

A. Experimental setup

The experimental setup and analysis procedure are detailed in Refs. [6,7] and only an overview of the setup is given in this section.

In this article, we report on the study of electromagnetically induced fission of ^{234,235}U and ^{237,238}Np, using inverse kinematics at relativistic energies. At such energies, ions are mostly fully stripped and in this case the atomic number Z is equal to the charge state, Q. The latter is obtained from an energy loss (ΔE) measurement provided by a multisample ionization chamber (MUSIC [8]), after correction of the velocity dependence of ΔE. The mass A of the relativistic ion is determined by its magnetic rigidity, $B\rho$: $A/Q \propto B\rho/\beta\gamma$,
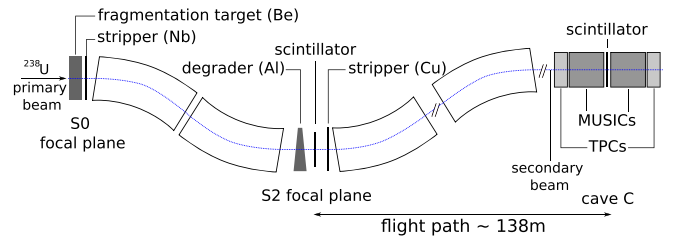

FIG. 1. Schematic view of the FRS and of the first part of the setup, employed to separate and identify the secondary beams of interest. Figure not to scale.

with the reduced velocity, β, and the Lorentz factor, γ. The magnetic rigidity is determined by tracking the ion through a magnetic field, based on measurements of the horizontal position, x, and the corresponding angle, θ. Therefore, by combining ΔE, $B\rho$, and time-of-flight (ToF) measurements with a sufficiently high accuracy, an isotopic identification in terms of Z and A can be obtained. With the R3B/SOFIA setup, such a measurement is possible on an event-by-event basis for the secondary beam of interest at the fragment separator (FRS, [9]) and for both fission fragments in coincidence at the high-energy experimental area of the GSI facility, Cave C, using the large acceptance dipole (ALADIN [10]) installed there. Figure 1 shows the part of the setup dedicated to the identification of the secondary beams. The beams are produced by fragmentation or charge-exchange reactions of a 1 A GeV primary ^{238}U beam on a beryllium target. Event by event, the ToF is measured along a 138-m-long flight path by two plastic scintillators located at the S2 focal plane and at the entrance of Cave C. Both scintillators also provide horizontal position measurements, based on the time difference between two photomultipliers mounted on the left and right sides of the scintillator. Two time-projection chambers (TPC [11]) and two multisampling ionization chambers from the Technical University of Munich (TUM-MUSIC [8]) were mounted at Cave C to complete this setup. The angle of the incoming ion is obtained using both TPC detectors. In contrast to the fission fragments, these very heavy ions can still carry one or two electrons. Therefore, two independent measurements of the ionic charge states, Q_1 and Q_2, are inferred from the energy-loss measurements by the first and second TUM-MUSIC detectors. The identification of the nuclear charge of the secondary beam is thus obtained (see Ref. [7] for details). Figure 2 presents the (Z vs A/Q) identification plot of the secondary cocktail beam. Thanks to an accurate measurement of the mass-over-charge ratio, the amount of uranium ions misidentified as protactinium ions, less than 10% (see the tail in Fig. 2 toward one charge lower), is further reduced compared to the amount of correctly identified atomic numbers. Figure 3 is a schematic view of the experimental setup at Cave C. It allows for the coincident identification of the nuclear charge and mass numbers of both fission fragments, with an average detection efficiency of 63%. This value was evaluated from a full Monte Carlo simulation (see Ref. [6] for all details). The secondary beam from the FRS has an energy at the entrance of the cave of about 700 A MeV. Coulomb fission is induced in flight in uranium and lead targets mounted
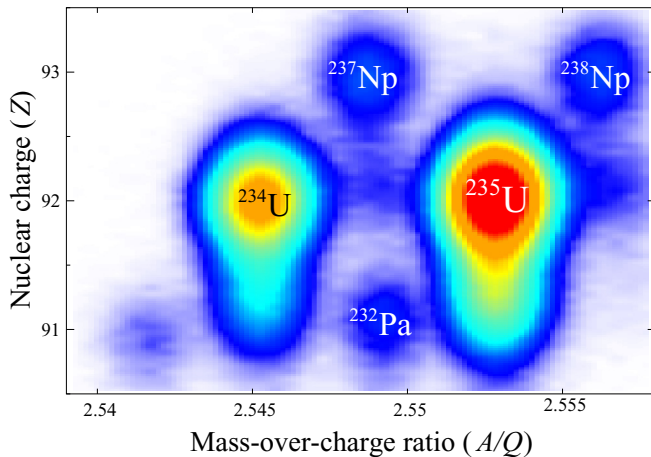
FIG. 2. Identification plot of the radioactive secondary beam for a sample of the recorded statistics.

as cathodes in an active target (see Ref. [6] for details). The fission fragments are emitted in the forward direction, within a narrow cone of 40 mrad at most, due to the relativistic boost from the secondary actinide beam. The identification of each fission fragment is obtained, similar to the identification of the secondary beam, with the ΔE-ToF-$B\rho$ technique. The energy loss is measured by the Twin-MUSIC, an ionization chamber consisting of two identical and independent chambers, sharing a common central cathode. Each fragment passes one half of the chamber, where its energy loss and horizontal angle are determined. Position measurements upstream and downstream the dipole magnet are performed with multiwire proportional chambers (MWPC [12]). The ToF of the fission fragments is obtained between the start scintillator and a time-of-flight wall [13], located at the very end of the spectrometer.

The measured atomic number distribution of the fission fragments is presented in the top panel of Fig. 4. It has a resolution of 0.35 charge units given in full width at half maximum (FWHM). The mass distribution, presented in the bottom panel of Fig. 4, is measured with a resolution varying from 0.59 mass units, FWHM, for the lighter fission fragments up to 0.8 mass units, FWHM, for the heavy fission fragments.

FIG. 4. Measured atomic-number distribution (a) and mass distribution (b) of the fission fragments produced by Coulomb-induced fission of ^{235}U. For details see text.

B. Fission reactions

In order to select only fission reactions, the data acquisition system is triggered when two ions are detected within 100 ns in the time-of-flight wall. However, two interaction mechanisms, leading to fission, may take place when the secondary beam interacts with a target nucleus. For the larger impact parameters, the interaction results in a Coulomb interaction between the high-energy actinide beam and the target nuclei, leading to the exchange of a virtual photon. This leads to the
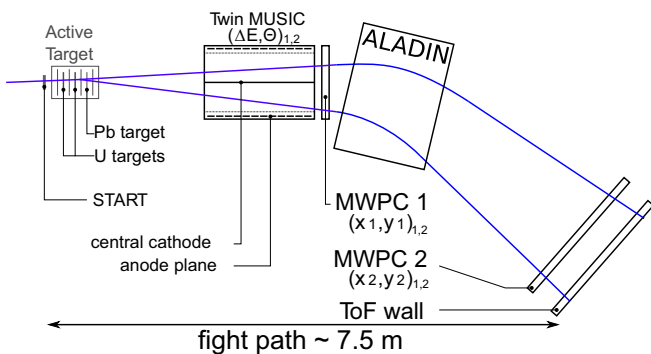

FIG. 3. Schematic view of the R3B/SOFIA setup located at Cave C and used for the coincident identification of both fission fragments in terms of their nuclear mass and charge. Figure not to scale.
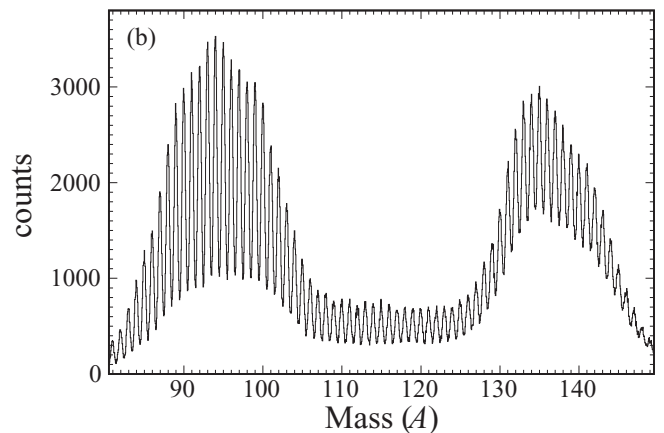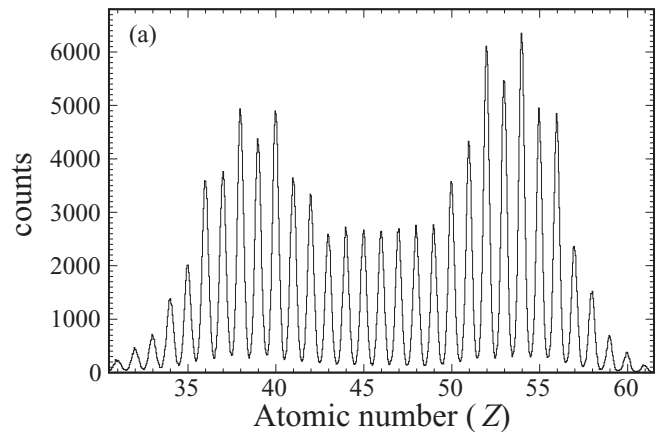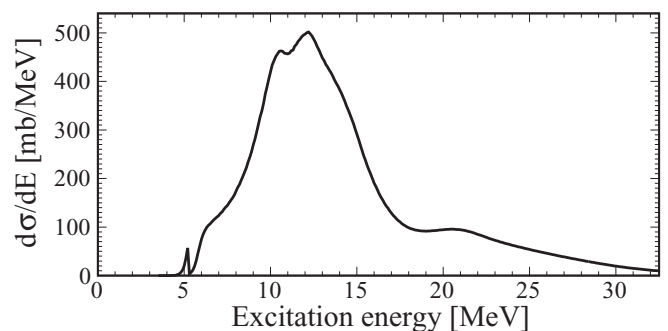

FIG. 5. Calculated excitation function of Coulomb-induced fission reaction of a 555 A MeV ^{235}U beam impinging a ^{238}U target.

TABLE I. Cross section and mean excitation energy for each studied Coulomb-induced fission reaction, calculated with a beam energy of 555 A MeV in the center of the target.

Beam	$\sigma_{\gamma,f}$ [b]	$\langle E^*_{\gamma,f} \rangle$ [MeV]
^{234}U	4.0	13.6
^{235}U	3.6	13.9
^{238}U	2.0	14.7
^{237}Np	4.8	13.5
^{238}Np	4.5	13.7

excitation of multipole resonances, mainly the giant dipole resonance. The calculation of the excitation function at fission is discussed in detail in Refs. [6,7]. The excitation energy of the electromagnetically induced fission of a ^{235}U beam at 555 A MeV in the center of a ^{238}U target is relatively low, as illustrated in Fig. 5. It covers a range from 5 to 30 MeV, with a mean value around 14 MeV (see Table I). Such an excitation energy is typically that of actinide nuclei after the absorption of a neutron of about 7–9 MeV, depending of the neutron binding energy [6,7].

If the impact parameter between the target and the projectile nuclei is small, a fragmentation reaction occurs. A number of nucleons is removed from the projectile, and the excitation energy of the resulting prefragment covers a large range up to hundreds of MeV. The de-excitation channels include fission, possibly preceded by neutron and/or light-charged particle evaporation. These events are rejected in a two-step analysis process. In the first step, only events where the sum of the nuclear charges of the two fission fragments (Z_{sum}) is equal to the nuclear charge of the fissioning nucleus (Z_{CN}), are analyzed. Yet, a fraction of the fragmentation-fission events remains, where only neutrons are removed during the fragmentation phase. This component cannot be removed on an event-by-event basis, but can be subtracted, in a second step, using data on fission in light-Z materials, such as aluminium (anodes of the active target) and glass (exit window of the second MUSIC detector). Table II provides for each fissioning nucleus, the number of fully reconstructed registered events, in which $Z_{\text{sum}} = Z_{\text{CN}}$ (no charged particle emission). The full subtraction procedure is described and illustrated in Ref. [6].

III. COULOMB-INDUCED FISSION OF ^{234,235}U

A. $Y(Z)$: Elemental yields

The elemental yields with their associated uncertainties, measured for ^{234,235}U(γ,f), are represented in Fig. 6(a), and
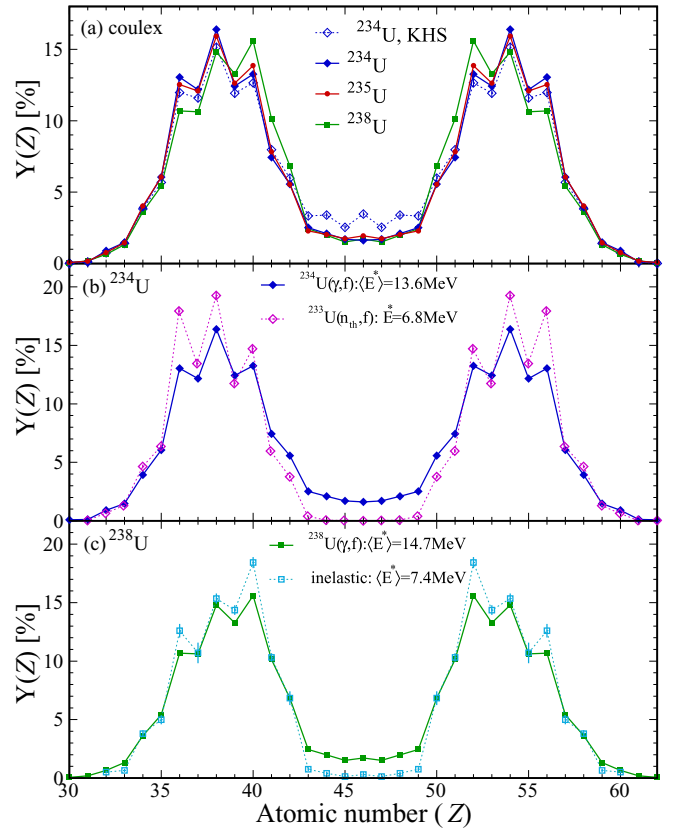
FIG. 6. (a) Elemental yields, measured for ^{234,235,238}U(γ,f) in this work and Ref. [6] (full lines) and as reported in Ref. [4] (dashed line, labeled KHS). Results for the fissioning nuclei ^{234,238}U are also compared, respectively, in panels (b) and (c), to data sets at lower excitation energies (dotted lines) obtained by Quade *et al.* [14] for ^{234}U and Ramos *et al.* [15] for ^{238}U.

the numerical values are given in the Supplemental Material [16]. Thanks to the very high efficiency, the full acceptance of the setup and the good Z resolution, the uncertainties are dominated by the statistics. For the most populated reaction, ^{235}U(γ,f), the yields are thus obtained with an unprecedented accuracy, below 1% for asymmetric fission and below 4% for symmetric splits.

Coulomb-induced fission was measured previously for ^{234}U [4]. The comparison shown in Fig. 6(a) is consistent but exhibits higher yields for symmetric fission in this former experiment. This feature is understood as coming from the lower accuracy in Ref. [4] in the subtraction of the nuclear-fragmentation component.

TABLE II. Number of fully reconstructed fission events. The fission events from the anodes and glass are used for the nuclear contribution subtraction, as explained in Ref. [6].

Nuclide	Targets	Anodes	Glass
^{234}U	248 450	3108	12 487
^{235}U	1 533 665	18 177	83 130
^{237}Np	14 474	175	599
^{238}Np	50 461	552	2596

TABLE III. ^{234,235,238}U(γ,f): 5-Gaussians fits on $Y(Z)$.

	Fission mode	^{234}U	^{235}U	^{238}U
ST1	Constant	1.82	3.52	6.79
	$\langle Z_L \rangle, \langle Z_H \rangle$	40.67,51.33	40.40,51.60	40.38,51.62
	σ_{ST1}	1.21	1.15	1.27
ST2	Constant	14.41	13.86	12.10
	$\langle Z_L \rangle, \langle Z_H \rangle$	37.85,54.15	37.72,54.28	37.70,54.30
	σ_{ST2}	2.35	2.29	2.30
SL	Constant	1.61	1.79	1.56
	σ_{SL}	4.00	4.00	4.00

Figure 6(b) shows the comparison of the elemental yields between Coulomb-induced fission of ^{234}U and thermal-neutron induced fission of ^{233}U [14]. Such a comparison demontrates the effect of the increased excitation energy of the fissioning nucleus, since Coulomb-induced fission populates the fissioning nucleus with an excitation energy, which is about 8 MeV higher than for thermal-neutron induced fission. Consequently, the SL symmetric mode is more likely to be populated in the data presented here, and the even-odd staggering appears to be considerably reduced, as discussed in detail in the following section (see Sec. III B). The same conclusions are reported by Ref. [17] and illustrated by Fig. 6(c). It compares the elemental yields measured for ^{238}U(γ,f) with the yields of the same ^{238}U compound nucleus produced by inelastic scattering on an carbon target with an average excitation energy of 7.4 MeV. Finally, along the uranium isotopic chain, the distribution of the fission fragments measured within this work, at a similar excitation energy, is rather stable for symmetric scission, but the maximum for asymmetric scission changes from $Z_H = 52$ in ^{238}U(γ,f) to $Z_H = 54$ in the lighter isotopes. This originates from a decrease of the influence of the ST1 fission mode when the N/Z ratio of the compound nucleus moves away from that of ^{132}Sn. In order to emphasize the contribution of each fission mode, the elemental yields have been fitted with a set of five Gaussian functions according to Ref. [18]. Numerical values of the fits are given in Table III. As illustrated in Fig. 7, the ST1 fission mode becomes more prominent if the number of nucleons in the compound nucleus increases and the ST2 mode becomes correspondingly weaker.
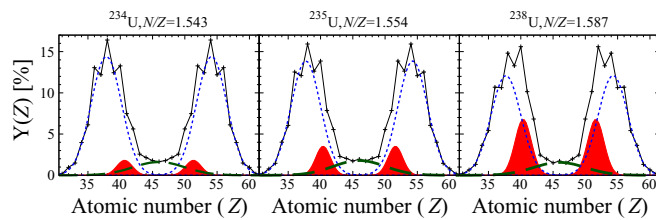

FIG. 7. Evolution of the elemental yields along the uranium isotopic chain for ST1 (filled red areas), ST2 (blue dotted lines), and SL (green dashed lines) fission modes, determined with a five-component fit of the measured elemental yields (black lines). The N/Z ratio of the compound nuclei should be compared to that of ^{132}Sn which has $N/Z = 1.64$.

B. Proton even-odd staggering

Figure 6 also shows an enhancement of the even-Z fission fragments. This excess yield can be quantified, both globally and locally.

The global even-odd effect (G_{eo}) is calculated as follows: $G_{eo} = (Y_e - Y_o)/(Y_e + Y_o)$, where Y_e (Y_o) is the total yield of fragments with an even (odd) number of protons. The values for all studied uranium fissioning systems are listed in Table IV, as well as the value for Coulomb-induced fission of ^{234}U, measured in Ref. [4]. The latter agrees with this work. In order to demonstrate the influence of the excitation energy on this even-odd staggering, other data from fission of the isotopes ^{234,238}U have also been included. In Ref. [14], thermal-neutron induced fission was studied, which populates the ^{234}U compound nucleus with an excitation energy of 6.8 MeV. Reference [17] reports on fission of the ^{238}U compound nucleus, populated by inelastic scattering with an average excitation energy of 7.4 MeV. Given that the excitation energy for the compound nuclei ^{234,238}U in these data is 7 MeV lower compared to the data from Coulomb-induced fission, the global even-odd staggering increases for them by 78% and 60%, respectively.

The local even-odd staggering (δ_{eo}) is obtained according to the approach proposed in Ref. [19]:

$$\delta_{eo}(Z + 1.5) = \left(-\tfrac{1}{8} \right)^{Z+1} \{ (\ln Y_{Z+3} - \ln Y_Z) \\ -3 \times (\ln Y_{Z+2} - \ln Y_{Z+1}) \}. \tag{1}$$

It gives an estimate of the local fluctuation of the yields compared to a Gaussian distribution. Figure 8(a) shows the local even-odd staggering, as a function of the atomic number. Only half of the distribution is depicted since the Z distribution is intrinsically symmetric. Globally, for the three fissioning uranium isotopes, the even-odd staggering is lower in the symmetric region, populated by the SL mode. The latter is dominantly fed by the high-energy part of the excitation energy distribution represented in Fig. 5. Therefore, in Coulomb-induced fission, the SL mode is populated with higher excitation energy than the asymmetric modes and more energy is available to break pairs of protons. In contrast, for asymmetric regions, the local even-odd effect increases steadily with the asymmetry.

Three local variations, marked in gray in the figure, are observed around $Z_H = 50$, $Z_H = 52$, and $Z_H = 56$. The yields for these even-Z elements are higher than expected for

TABLE IV. Numerical values of the global proton even-odd staggering measured in ^{234,235,238}U(γ,f) (this work and Refs. [4,6]), in ^{233}U(n_{th},f) [14] and in fission of ^{238}U produced by inelastic scattering [17].

Reaction	$G_{eo}(Z)$ [%]	$\langle E^* \rangle$ [MeV]
^{233}U(n_{th},f) [14]	21.8 ± 0.5	6.8
^{234}U(γ,f) [4]	12.5 ± 1.0	13.6
^{234}U(γ,f)	12.2 ± 0.4	13.6
^{235}U(γ,f)	11.5 ± 0.2	13.9
^{238}U(γ,f) [6]	10.1 ± 0.1	14.7
^{238}U(^{12}C, ^{12}C$'$) ^{238}U* [17]	16.2 ± 1.6	7.4

even-odd pairing and probably directly related to the fission modes. Indeed, they are exactly located at the expected proton shells responsible for the asymmetric modes: the first variation located at $Z_H = 50$ corresponds to the ST1 mode, and the location of the two others is completely consistent with the interpretation of the ST2 mode caused by the influence of octupole-deformed proton shells located at $Z_H = 52$ and $Z_H = 56$ [5]. As the excitation energies for the different reactions are similar (see Table I), and, considering that the excitation energy needed to break a pair of nucleons is not changing significantly from ^{234}U up to ^{238}U, the ratio of the even-odd staggerings between ^{234,235}U and ^{238}U, as represented in Fig. 8(b), allows us to suppress the influence of the excitation energy on the even-odd staggering in order to obtain an estimate of the evolution of the weight of each fission mode. As previously seen in the elemental yields, the influence of $Z_H = 50$, corresponding to the ST1 mode is stronger for the fission of ^{238}U, since both ratios are lower than

one (indicated with a dotted line). In contrast, the influence of $Z_H = 52$ and $Z_H = 56$ corresponding to the ST2 mode is weaker. Due to the overlap with the SL mode, it is not possible to learn more about the ST1 fission mode. In contrast, the ST2 mode can be discussed in more detail. First, the effect of both components of the ST2 mode can be decoupled: It seems that from ^{238}U to ^{234}U, the increasing influence of this mode is larger for $Z_H = 52$ than for $Z_H = 56$. Then, the effect of the excitation energy can be investigated, based on Fig. 9. The latter exhibits in the upper panel the comparison of the local even-odd staggering between Coulomb-induced fission of ^{234}U and thermal-neutron induced fission of ^{233}U [14], and in the lower panel the ratio of both quantities. As mentioned already, the even-odd staggering is considerably stronger on a global scale when the excitation energy decreases. It is unexpected that the ratio within the ST2 area is rather flat. This observation supports the hypothesis that the influence of the ST2 mode on the potential energy landscape does not change within this excitation-energy difference.
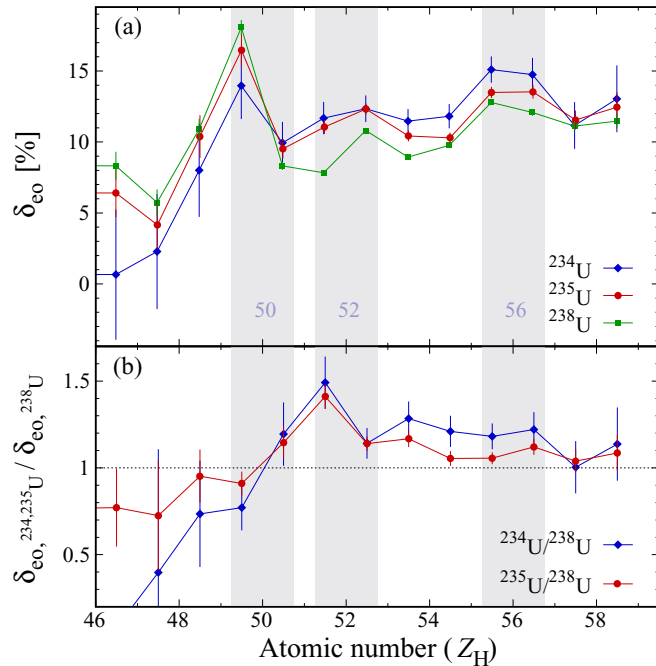

FIG. 8. (a) Proton local even-odd staggering measured in this work for ^{234,235,238}U(γ,f), represented with blue diamonds, red circles, and green squares, respectively. (b) Ratio between the local even-odd staggerings in ^{234,235}U(γ,f) and those in ^{238}U(γ,f).
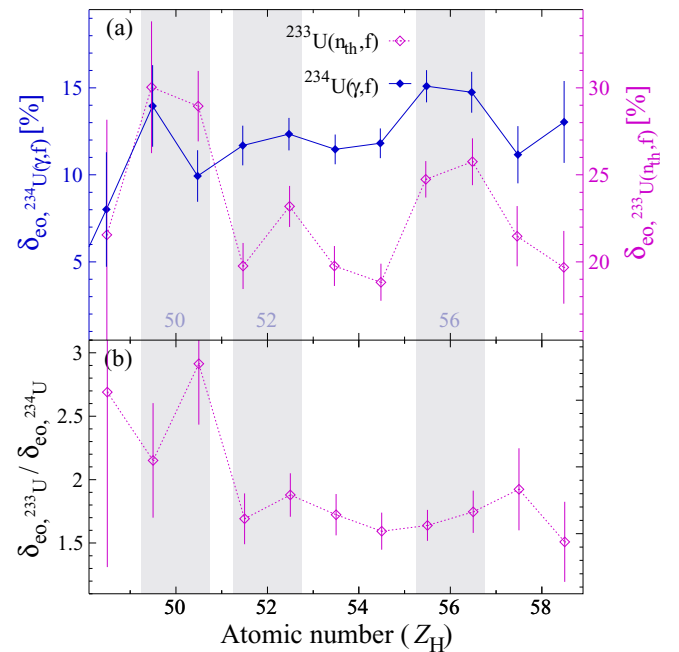

FIG. 9. (a) Comparison of the proton local even-odd staggering between ^{234}U(γ,f) (full blue diamonds, left axis) and ^{233}U(n_{th},f) (open purple diamonds, right axis [14]). (b) Ratio between the local even-odd staggering in ^{233}U(n_{th},f) [14] and ^{234}U(γ,f).

FIG. 10. (a) Isobaric yields, measured for ^{234,235,238}U(γ,f) in this work and in Ref. [6]. Results for the fissioning nuclei ^{234,238}U are compared in panels (b) and (c), respectively, to other data sets at lower excitation energies (dotted lines) measured by Quade *et al.* [14] and Martin *et al.* [20] for ^{234}U, and Ramos *et al.* [15] for ^{238}U.
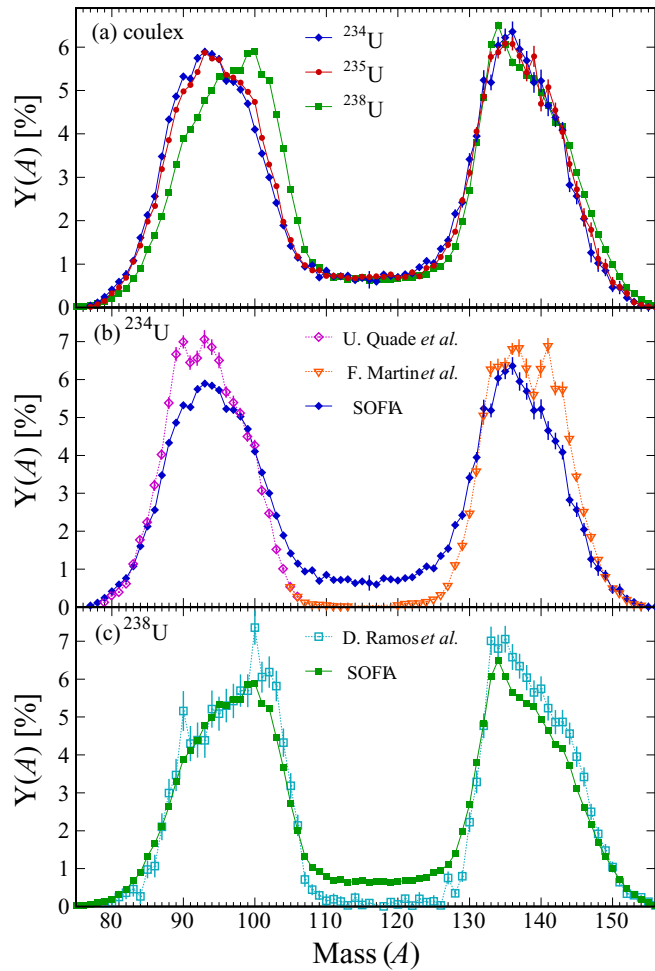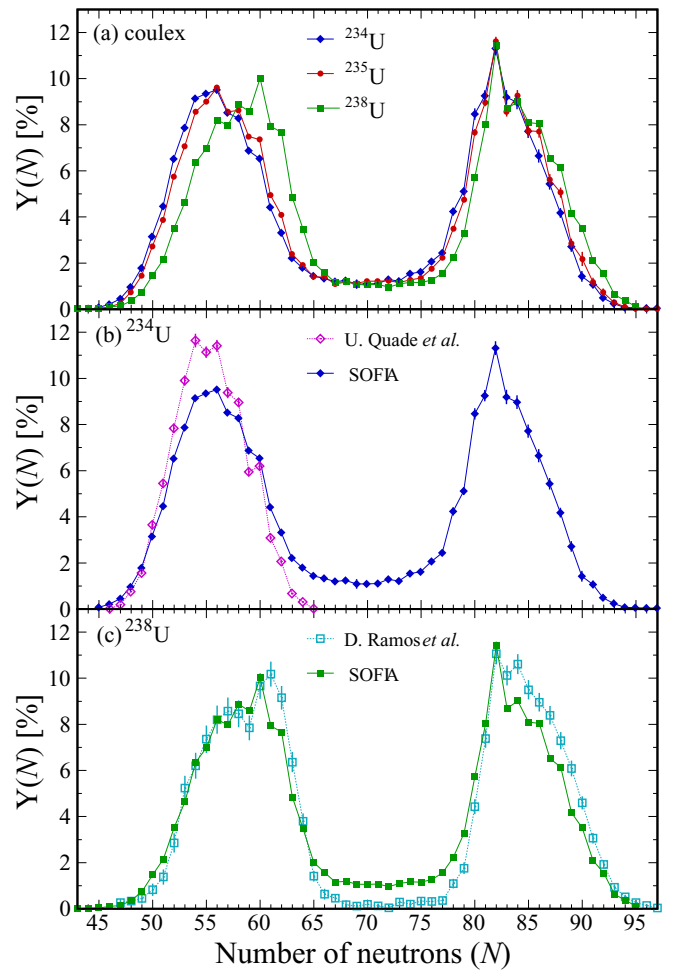

FIG. 11. (a) Isotonic yields measured for ^{234,235,238}U(γ,f) in this work and in Ref. [6]. Results for the fissioning nuclei ^{234,238}U are compared in panels (b) and (c), respectively, to other data sets at lower excitation energies (dotted lines), measured by Quade *et al.* [14] for ^{234}U and Ramos *et al.* [17] for ^{238}U.

C. $Y(A)$ and $Y(N)$: Isobaric and isotonic yields

The isobaric and isotonic yields are presented in Figs. 10(a) and 11(a), respectively, and their numerical values are reported in the Supplemental Material [16]. For both isobaric and isotonic yields, the peak of the heavier fragments remains approximately centered at the same position for all three uranium isotopes, while the peak of the lighter fragments moves accordingly to compensate for the variation in the total number of neutrons of the fissioning systems. Figures 10 and 11 also present a comparison of the isobaric and isotonic yields measured for the ^{234,238}U fissioning nuclei in this experiment, with data obtained at lower excitation energy. The latter, thermal neutron-induced fission of ^{233}U [14,20] and fission of ^{238}U produced by inelastic scattering in inverse kinematics [15] show a more asymmetric behavior; the symmetric valley is depleted. In Coulomb-induced fission data, given that the excitation energy is around 7 to 8 MeV higher, the SL symmetric mode populates the range $110 \leqslant A \leqslant 130$. Nevertheless, looking at the ^{234}U data, a fine structure is observed

for the light fragment group in the isobaric yields. This fine structure is very similar at both excitation energies, indicating that the underlying effects responsible for the enhancement of the yields at $A = 90$ and $A = 92$–95 are preserved over the large excitation energy range. The authors of Ref. [17] came to the same conclusion when they discussed isotonic yields measured for fission of ^{238}U. Again, the enhancement of the yields at $N_{\rm L} = 60$ and $N_{\rm H} = 82$ is well preserved.

The fission fragments are identified by the R3B/SOFIA setup after prompt-neutron emission but before any delayed decay. Therefore, the understanding of the measured isotonic and isobaric yields is more complex than the one of the measured elemental yields, since the neutron evaporation stage must be considered in the interpretation of the results. Global neutron even-odd staggering probes the prominent role of the neutron evaporation stage. Table V presents the comparison of the $G_{\rm eo}(N)$ values for Coulomb-induced and thermal-neutron induced fission. In contrast to $G_{\rm eo}(Z)$, the influence of the excitation energy appears to be weak, indicating that the neutron separation energy of the last neutron is decisive in the

TABLE V. Numerical values of the global neutron even-odd staggering measured for ^{234,235,238}U(γ,f) and compared to thermal-neutron induced fission of ^{233}U [14].

Nuclide	$G_{\mathrm{eo}}(N)$ [%]	$\langle E^* \rangle$ [MeV]
^{233}U(n_{th},f) [14]	5.5 ± 0.7	6.8
^{234}U(γ,f)	3.4 ± 0.5	13.6
^{235}U(γ,f)	5.4 ± 0.4	13.9
^{238}U(γ,f) [6]	5.1 ± 0.2	14.7

observed even-odd staggering as studied in Ref. [21]. Even-odd proton and neutron staggering might be similar at scission, but the neutron even-odd staggering might be significantly washed out during de-excitation of the fragments by neutron evaporation. This weaker even-odd staggering, leading to an enhanced production of the even-N fission fragments, is well observed for all isotonic yields presented in Fig. 11. In addition to this staggering, a strongly enhanced production of the isotone $N = 82$ is clearly seen for all three fissioning isotopes. This is due to the magicity of $N = 82$, which acts as a trap during the neutron evaporation process due to its high neutron separation energy.

D. $Y(Z, N)$: Isotopic yields

Isotopic fission yields obtained for ^{234,235,238}U(γ,f) are presented in Fig. 12. The data cover the whole fission fragment charge range from $Z = 30$ to $Z = 60$. Error bars in the figure indicate statistical uncertainties, illustrating the level of accuracy obtained with the R3B/SOFIA setup. For the light fission fragment group, uncertainties are mostly below 2.5%. For the heavy fission fragment group and at symmetry, uncertainties are below 7% for the most probable isotopes. For very asymmetric fission, the heavy fission fragments ($Z \geqslant 57$) uncertainties are below 20%. All numerical values obtained for isotopic yields for ^{234,235}U(γ,f) are given in the Supplemental Material [16]. Numerical values for ^{238}U(γ,f) were previously reported in Ref. [6]. It was mentioned before that the most abundant elements vary from ($Z_L = 38$, $Z_H = 54$) in ^{234,235}U(γ,f) to ($Z_L = 40$, $Z_H = 52$) in ^{238}U(γ,f). With Fig. 12, the most abundant isotope is identified to be ($Z = 54$, $N = 82$) and ($Z = 52$, $N = 82$), for fission of ^{234,235}U and ^{238}U, respectively. This explains the shift of two mass units for the maximum of the mass yields from $A_H = 136$ to $A_H = 134$.

Finally, it appears that for all elements, the isotopic distribution follows a Gaussian-like distribution, covering eight to 12 neutron numbers. Elements $Z_H = 49$ (indium) and $Z_H = 50$ (tin) show a quite different behavior, with an asymmetric shape, as illustrated in Fig. 13. Indium is centered at $N = 73$ and shows a tail which extends up to $N = 80$. In contrast, tin isotopes are centered around $N = 78$, with a tail which extends down to $N = 72$. Therefore, a shift of just one Z unit causes a shift in neutron number of five units. The role of the doubly closed shell in the vicinity of ^{132}Sn on asymmetric fission was underlined already in the introduction, and this is an experimental confirmation of its importance. The strong difference in the mean N value between $Z = 49$ and $Z = 50$ is linked to the attractive power of the ^{132}Sn region and the transition from the symmetric SL to the asymmetric ST1 fission

mode. This effect is even larger, as previously seen in Fig. 7, in the case of ^{238}U(γ,f). The tails observed in the isotonic distributions of indium and tin are the signatures of SL and ST1 fission modes. Element indium is mainly produced by the SL channel, but also by the ST1 channel which causes a tail extending towards higher N values. Element tin, on the other hand, is mainly produced by the ST1 channel, and the residual contribution of the SL mode causes a tail toward lower N values.

E. Prompt-neutron multiplicity

Since the experimental setup measures the masses of the compound nucleus (A_{CN}) and fission fragments (A_{FF_1} and A_{FF_2}) on an event-by-event basis, the total prompt-neutron multiplicity (ν_{tot}) is obtained by $\nu_{\mathrm{tot}} = A_{\mathrm{CN}} - A_{\mathrm{FF}_1} - A_{\mathrm{FF}_2}$. All numerical values of $\langle \nu_{\mathrm{tot}} \rangle$ are given in the Supplemental Material [16].

The average value $\langle \nu_{\mathrm{tot}} \rangle$ can be plotted as a function of the atomic and/or neutron number of one fission fragment, as shown in Figs. 14 and 15. Such correlations probe the configuration at scission. One observes in Fig. 14 that the total prompt-neutron multiplicity ranges from three to six neutrons, with the highest multiplicity occurring for symmetric fission events. This symmetric configuration corresponds to the SL fission mode. The associated path from saddle to scission is very long, and both fission fragments show a high quadrupolar deformation. After scission, the fragments relax into their ground-state shape, and the deformation energy is converted into excitation energy. This excitation energy is then released through prompt-neutron emission, and the multiplicity is thus much higher than in asymmetric fission. Figure 14(b) surprisingly shows that $\langle \nu_{\mathrm{tot}} \rangle$, averaged on the isotonic chain, is rather stable for the light-fragment group around 3.8, for the isotones below $N_L = 56$. On the opposite side, $\langle \nu_{\mathrm{tot}} \rangle$ decreases sharply for the heavy-fragments group above $N_H = 82$.

For the ^{234,235}U(γ,f) reactions, those which were obtained with higher statistics, the average value of the *total* prompt-neutron multiplicity is plotted as a function of the atomic and neutron numbers of *one* fission-fragment, in Fig. 15. For each element, lower neutron numbers correspond to higher prompt neutron multiplicity, which simply describes that the lower postemission neutron number of the fragments correlates with more important prompt-neutron emission. This is confirmed for all elements, except for molybdenum ($Z_L = 42$), and to some extent technecium ($Z_L = 43$). Both the asymmetric ST1 and the symmetric SL modes contribute to the production of these elements, but their influences drive the neutron multiplicity in opposite directions. In the asymmetric mode, higher
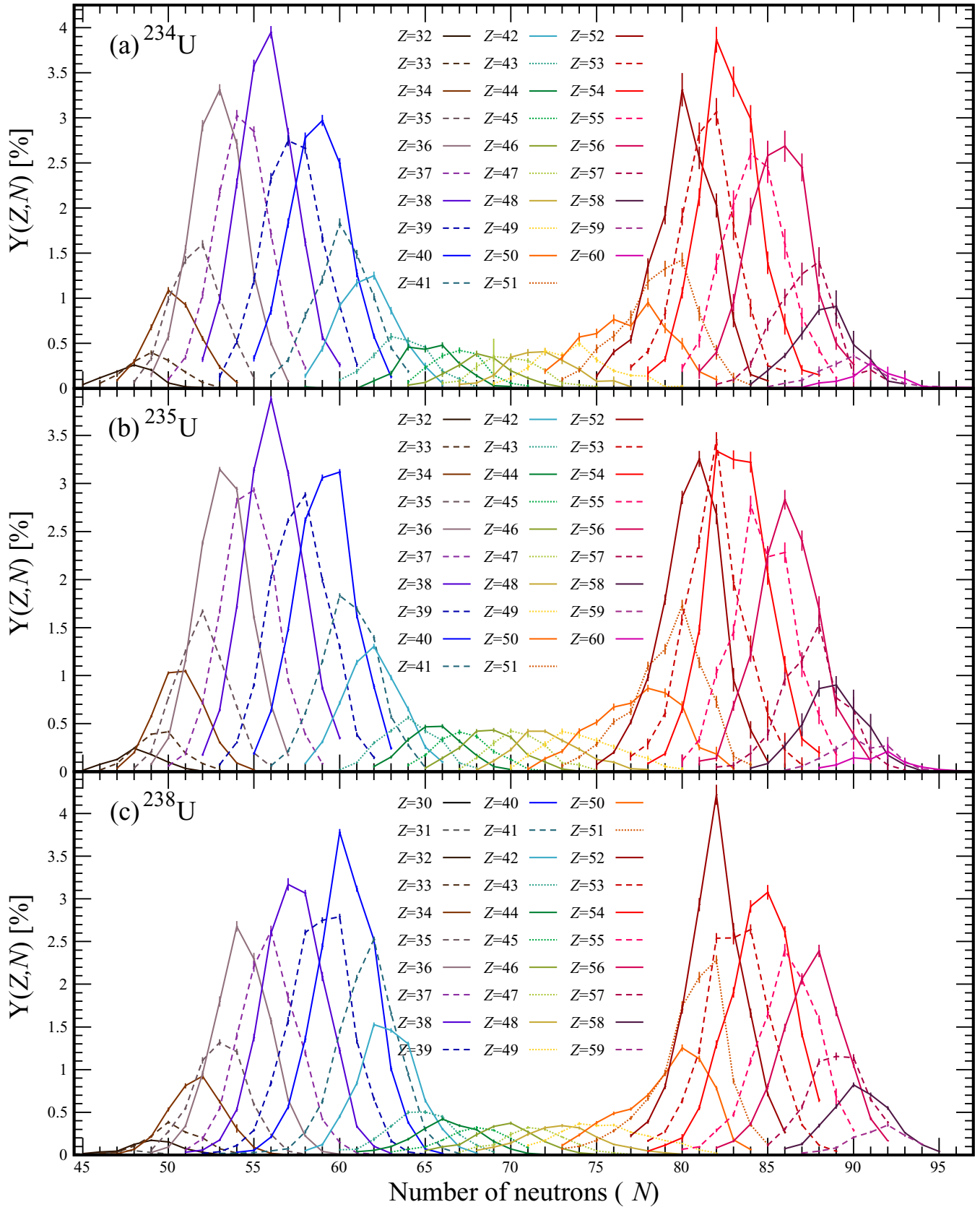
FIG. 12. The isotopic yields measured for ^{234,235}U(γ,f) are presented in panels (a) and (b), respectively. For comparison purpose, the isotopic yields measured for ^{238}U(γ,f) [6] obtained with the same R3B/SOFIA setup are presented in panel (c).
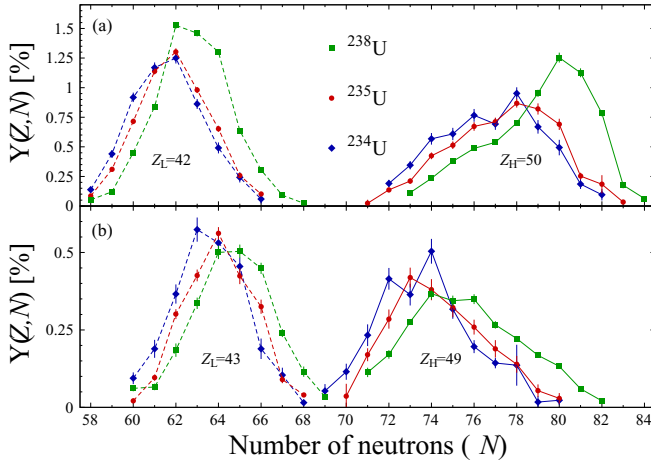
FIG. 13. Isotopic yields measured for Coulomb-induced fission of ^{234}U (blue diamonds), ^{235}U (red circles), and ^{238}U (green squares [6]) for two fission fragment pairs: $(Z_L = 42, Z_H = 50)$ in panel (a) and $(Z_L = 43, Z_H = 49)$ in panel (b). Yields of the light (heavy) fragments are plotted with dashed (full) lines.

prompt-neutron multiplicity corresponds to lower number of neutrons in the fission fragments. However, as the latter increases, the SL mode plays a larger role and tends to increase the prompt-neutron multiplicity. Of course, this is not seen for the complementary element tin $(Z_H = 50)$, which is also produced through both the ST1 and SL modes, because in this case the contribution of the SL mode increases as the number of neutrons decreases. Instead, we observe a variation in the slope: It is stronger from $N = 71$ to $N = 77$ and then becomes softer.
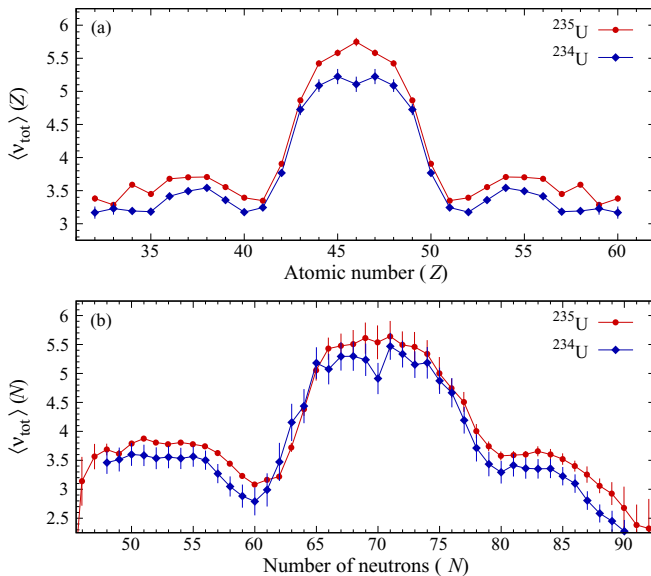

FIG. 14. Average value of the total prompt-neutron multiplicity as a function of atomic number and neutron number, respectively in panels (a) and (b), of one fission fragment measured after prompt-neutron evaporation, for Coulomb-induced fission of ^{234,235}U represented with blue diamonds and red circles, respectively.

IV. COULOMB-INDUCED FISSION OF ^{237,238}Np

As shown in Fig. 2, beams of the odd-Z ^{237,238}Np were also present in the same FRS setting but with much less statistics (see Table II of Sec. II B). This leads to higher statistical uncertainties. Nevertheless, the elemental yields measured for ^{237,238}Np(γ,f) are shown in the lower panel of Fig. 16 and their numerical values are given in the Supplemental Material [16]. They are obtained for the most populated elements in asymmetric fission with uncertainties below 5% and for symmetric fission with uncertainties below 15%. Figure 16 also shows that the most populated fission-fragment pair is not identical for the two fissioning systems. Whereas the elemental yields are enhanced for the $(Z_L = 39, Z_H = 54)$ pair of fission fragments, with an even-Z_H fission fragment for ^{237}Np(γ,f), it is the $(Z_L = 40, Z_H = 53)$ pair characterized by an even-Z_L which is enhanced for the fission of ^{238}Np. Finally, charge conservation in the scission process enforces the global even-odd staggering to be zero. However, some fine structure exists in the local even-odd staggering, as shown in the upper panel of Fig. 16. For both neptunium nuclides, δ_{eo} is positive, showing an enhanced production of even-Z fission fragments around $Z_H = 50$, but also for the very asymmetric light fragment group.

Figure 16 also compares elemental yields measured in this work with those for fission of ^{239}Np produced at a lower average excitation energy of 7.5 MeV by the transfer reaction ^{12}C$(^{238}$U, ^{239}Np$)^{11}$B [15,17]. Two effects are observed in this comparison which are fully consistent with what has already been highlighted for the fission of uranium isotopes: As the excitation energy decreases, the symmetric SL mode becomes less likely, and the amplitude of the even-odd staggering if it is locally nonzero is increasing. This is particularly clear for the amplitude of the local even-odd staggering around $Z = 50$, which is also larger for fission of ^{239}Np, which has an N/Z value closer to that of ^{132}Sn.

Numerical values of the isobaric and isotonic yields are given in the Supplemental Material [16]. The most populated asymmetric yields are obtained with uncertainties around 5% (10%), and the symmetric yields with uncertainties around 30% (40%) for the fission of ^{238}Np $(^{237}$Np$)$.

Finally, despite the weaker statistics, the isotopic yields were also measured. For the most populated fission fragments, the uncertainties obtained for the fission of ^{237,238}Np are below 12% and 8% in the light fragment group, respectively, and between 10% and 25% among the heavy fragments. The full set of isotopic yields measured for Coulomb-induced fission of ^{237,238}Np are drawn and the numerical values are given in the Supplemental Material [16].

V. MEAN VALUES OF THE FISSION YIELDS

A. Mean values for asymmetric fission

The mean values of the atomic, neutron, and mass numbers of the light and heavy fragment groups have been extracted with a precision of 0.1 to 0.2 units. Each yield distribution is fitted with a sum of three Gaussian distributions. An additional constraint is added, in the multifit of the isotonic and isobaric yields, to ensure that the light and heavy components
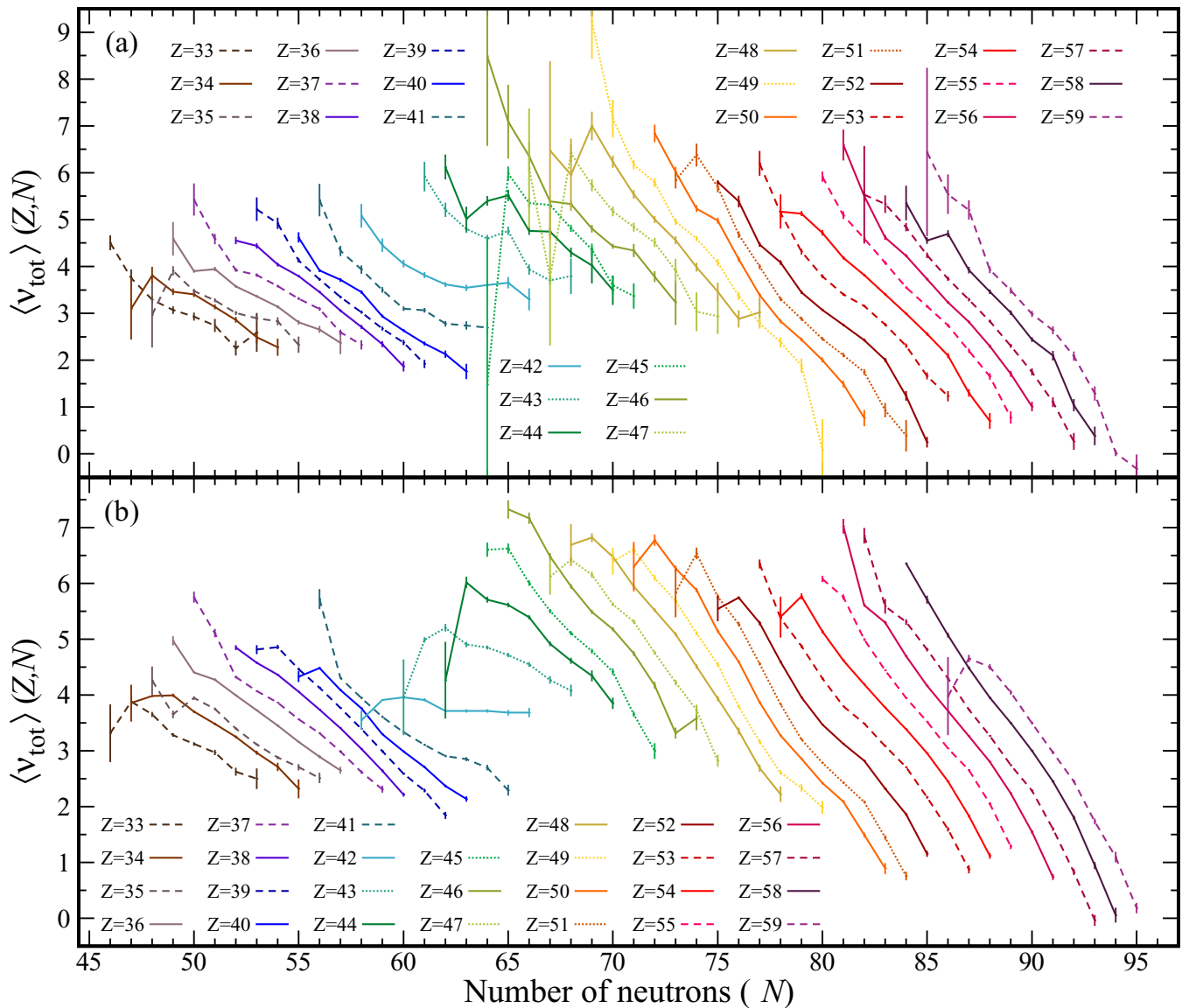
FIG. 15. For each element produced in ^{234,235}U(γ,f), the average value of the measured total prompt-neutron multiplicty is presented as a function of the number of neutrons in panels (a) and (b), respectively.

show the same integral yields. Indeed, for these yields, the width of the heavy component is larger than that of the lighter one. A comparison of the results obtained for the fission of the uranium and neptunium isotopes is given in Table VI for the light and heavy fragment groups.

For these fissioning systems, the heavy fragments play a prominent role in asymmetric fission. Indeed, the heavy peak remains approximately at the same position, while the lighter peak positions compensate for the variation in proton and neutron numbers of the compound nucleus. This feature has long been known. Asymmetric fission was found actually in the uranium to curium region to be characterized by heavy fission fragments distributed around a mean mass of $\langle A_H \rangle \approx 138$–140, while the mean mass of the light fission fragments increases with the mass of the fissioning nucleus [22,23]. Then, from the systematic measurement of the elemental yields over a large region of the nuclide chart (up

to uranium), it has been found that the heavy peak shows an almost constant mean Z value [4]. This new set of data confirms this trend also for the fission of ^{237,238}Np.

B. Neutron excess

Figure 17 illustrates the measured neutron excess ratio, defined as the average neutron number per proton, i.e., $\langle N_{FF} \rangle / Z_{FF}$. Since the measurement takes place after prompt-neutron evaporation, this ratio probes the interplay between the nuclear structure of the fragments and the prompt-neutron emission. Its evolution should be interpreted regarding not only the shell structure of the fragments which can populate preferentially some regions in the (Z, N) space, but also the prompt-neutron emission. Error bars are reported in the figures and are in most cases smaller than the symbol sizes. The evolution from lighter to heavier elements can therefore be
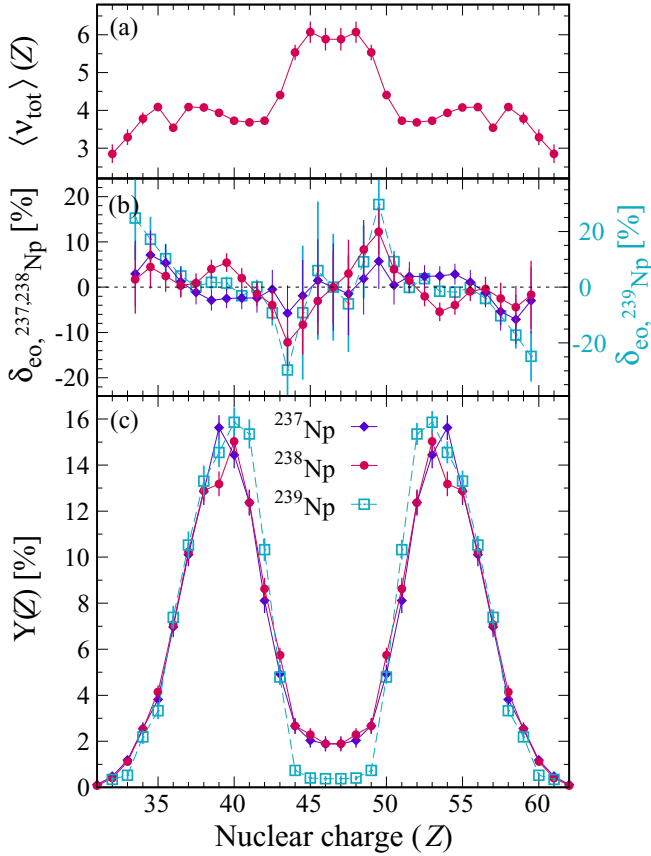
FIG. 16. (a) Total prompt-neutron multiplicity, (b) local even-odd staggering, and (c) elemental yields measured for ^{237,238}Np(γ,f) represented with diamonds and circles, respectively. The data are compared to the measurement of fission of ^{239}Np produced by a transfer reaction at $\langle E^* \rangle = 7.5$ MeV [15,17], represented with open squares.

FIG. 17. The average neutron number per proton $\langle N_{FF} \rangle / Z_{FF}$ measured (a) for the fission of ^{234,235}U (blue diamonds and red circles, respectively), and (b) for the fission of ^{238}Np.

accurately inferred and described. First, for very asymmetric fission, the neutron excess decreases strongly and steadily for light fission fragments from $Z_L = 32$ to $Z_L = 36$ and, for the heavy ones above $Z_H = 56$, with a smaller slope. Then, for the most populated asymmetric scission configuration, while the neutron excess decreases for the heavy fragments, it is flat from $Z_L = 36$ to $Z_L = 41$. Finally, as already observed in the low-energy fission of actinides in the same region, ^{238,239}U, ^{239}Np, and ^{240}Pu [6,17,24], the neutron excess steeply increases at $Z_L = 42$ before becoming smoother around the
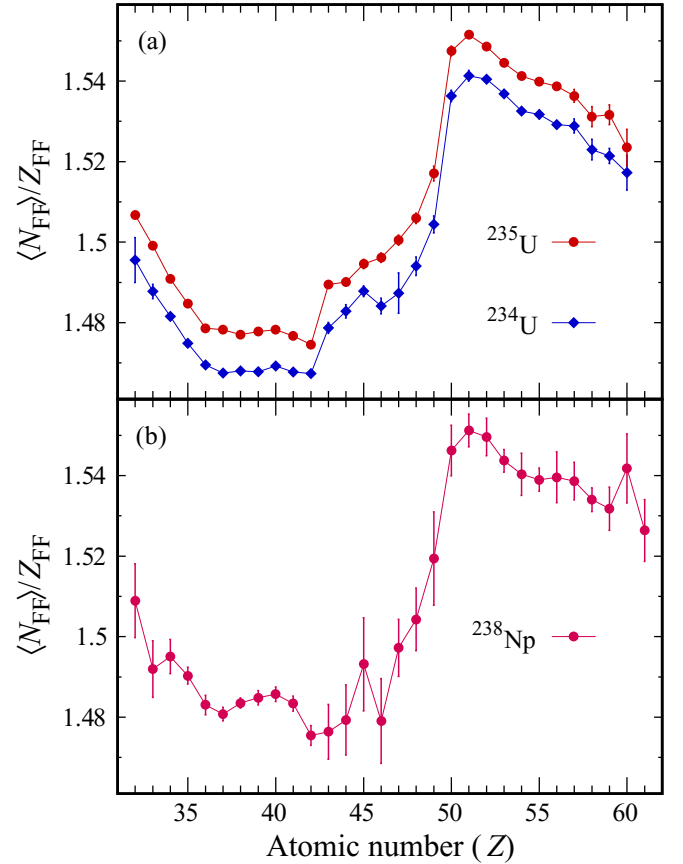
symmetric splitting and increases again suddenly and sharply at $Z_H = 50$. This phenomenon is another illustration of the population of the indium and tin isotopes by the population of the two different fission modes, namely the symmetric SL mode and the compact asymmetric ST1 mode. It confirms the conclusions already drawn from Fig. 13. The ST1 mode is strongest at the closed shell $Z_H = 50$, which populates primary fission fragments with a large number of neutrons, due to the additional influence of $N_H = 82$ spherical shell. As such heavy fission fragments are nearly spherical, the excitation energy originating from the deformation energy is small and the prompt-neutron evaporation is minimized. Both effects, the production of primary fragments with larger number of

TABLE VI. Average values of atomic, neutron, and mass numbers for the light and heavy fission fragments, measured for the Coulomb-induced fission of ^{234,235,238}U and ^{237,238}Np.

Nuclide	$\langle Z_L \rangle$	$\langle N_L \rangle$	$\langle A_L \rangle$	$\langle Z_H \rangle$	$\langle N_H \rangle$	$\langle A_H \rangle$
^{234}U [4]	38.2 ± 0.1			53.8 ± 0.1		
^{234}U	38.1 ± 0.1	55.7 ± 0.1	93.8 ± 0.1	53.9 ± 0.1	83.0 ± 0.1	136.9 ± 0.1
^{235}U	38.2 ± 0.1	56.1 ± 0.1	94.3 ± 0.1	53.8 ± 0.1	83.3 ± 0.1	137.0 ± 0.1
^{238}U [6]	38.6 ± 0.1	58.3 ± 0.1	96.6 ± 0.1	53.4 ± 0.1	84.2 ± 0.1	137.0 ± 0.1
^{237}Np	39.2 ± 0.1	57.6 ± 0.1	96.5 ± 0.2	53.8 ± 0.1	83.1 ± 0.2	137.1 ± 0.2
^{238}Np	39.3 ± 0.1	58.1 ± 0.1	97.5 ± 0.2	53.7 ± 0.1	83.3 ± 0.2	137.2 ± 0.2

neutrons and the weak prompt-neutron emission, maximize the neutron excess value at $Z_H = 50$.

VI. COMPARISON TO THE GEF MODEL

Calculations using the general description of fission observables (GEF) model [25–27] were also performed for the Coulomb-induced fission of ^{234,235}U, using GEF-2019V1.1 with the excitation energy distribution introduced in Sec. II B. In GEF, the prompt neutron multiplicity of each fragment is given by the excitation energy at scission and the deformation energy. The excitation energy of each fragment at scission is determined by the complete energy sorting process, where the intrinsic excitation energy available at scission is transferred to the heavy fragment. This process has its origin in the constant-temperature behavior of the fission-fragment level densities at low excitation energies [26,27].

Figure 18 presents the comparison of these results with some observables measured in this work: elemental and isotonic yields, neutron excess as defined in Sec. V B, and the total prompt-neutron multiplicity as a function of the atomic number of the fission fragments. The agreement between the experimental and calculated fission yields and neutron excess is rather good. A discrepancy of 0.2 neutrons is observed for the absolute values of the total prompt-neutron multiplicity. It might reflect the influence of a 1-MeV uncertainty on the mean value of the calculated excitation energy distribution (see Fig. 5). While the predicted $\langle N_{FF} \rangle / Z_{FF}$ ratio is consistent with our data for the heavy group, this discrepancy translates into a larger value of this predicted ratio for the light group. Note that the model reproduces well the evolution of all observables as a function of the charge asymmetry.

In calculations conducted in Sec. VII, we use GEF to infer the contribution of the neutron evaporation of the compound nucleus to $\langle \nu_{tot} \rangle$, thus obtaining $\langle \nu_{tot,FF} \rangle$, the average number of neutrons emitted by the fission fragments only. As expected, the contribution of the compound nucleus is found to be small: 5.4%, 7.8%, and 5.8% for Coulomb-induced fission of ^{234,235}U and ^{238}Np, respectively.

VII. FISSION OBSERVABLES AT SCISSION

In order to discuss the origin of the stability of the heavy fragment group, observables at the scission point are required. While proton numbers remain unchanged after scission, a variable number of neutrons are evaporated, thus blurring possible neutron-shell effects. The aim of this section is to extract from our experimental data set (postevaporation) the number of neutrons of the primary fission fragments (pre-evaporation).

Reference [4] was the first to propose Z shell effects as the main reason for the stability of the heavy group. However, at that time, the number of neutrons could not be measured and the $\langle N_{FF}^{pre} \rangle / Z_{FF}$ ratio at scission, prior to the neutron evaporation phase, was obtained based on the unchanged charge density (UCD) approximation. In this hypothesis, the mass-over-charge ratio is identical for both fission fragments and equal to that of the fissioning nucleus, as described in Sec. VII A. With our data, another approach can be used, since
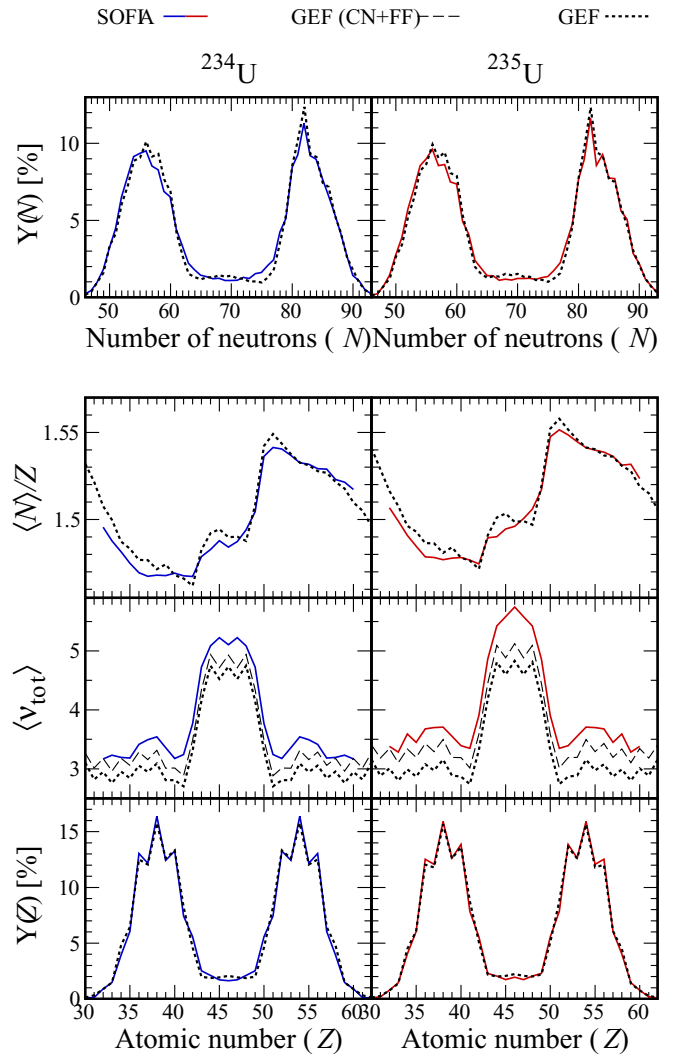

FIG. 18. Comparison between the fission yields, the neutron excess, and the total prompt-neutron multiplicity measured in this work (full colored lines) and calculated by the GEF code [25] (dotted black lines), for Coulomb-induced fission of ^{234,235}U in the left and right panels, respectively. Also plotted in the middle panels of the lower figure are the results of GEF for the neutron multiplicity (dashed black lines, $\langle \nu_{tot} \rangle$) including the neutrons emitted from the compound nucleus prior to fission and from the fission fragments.

the number of protons and neutrons of each secondary fission fragment (postevaporation) is measured in coincidence with the total prompt-neutron multiplicity per fragment partner, $\langle \nu_{tot} \rangle (Z_L, Z_H)$. Thus, by assuming certain sharing of $\langle \nu_{tot} \rangle$ between both fission fragments, the prompt-neutron multiplicity per fragment, $\langle \nu \rangle (Z_{L,H})$, can be obtained and then added to the number of neutrons of the secondary fission fragments to infer the number of neutrons of the primary fission fragments.

Two different methods are proposed to determine such a sharing and obtain $\langle \nu \rangle (Z_{L,H})$. The first one, based on a commonly used hypothesis which considers fission as an adiabatic process in a Fermi gas, is detailed in Sec. VII B. The second and more accurate one, which is described in Sec. VII C, is based on experimental results only. It combines our results

with previous data, measured at lower excitation energy for the two fissioning systems: ^{238}Np [28] and ^{234}U [29].

Finally, comparisons of results obtained from all approaches, UCD and the two methods to distribute $\langle\nu_{\text{tot}}\rangle$, and from the GEF calculations [25], are performed for the $\langle\nu\rangle$ values in Sec. VII D, for the neutron excess prior to the neutron evaporation phase in Sec. VII E, and for the average number of neutrons of the primary fission fragments in Sec. VII F.

A. UCD assumption

For numerous experimental studies, when only the mass or the atomic number of the fragments are measured, the UCD hypothesis is the only approach which can be used to infer the proton and neutron numbers of the fission fragments at scission. In the following, we compare this hypothesis with the other approaches. Therefore, $\langle N_{\text{FF}}^{\text{pre}}\rangle_{\text{UCD}}$, the average value of the neutron number of the fission fragments at scission can be obtained before neutron evaporation:

$$\langle N_{\text{FF}}^{\text{pre}}\rangle_{\text{UCD}}(Z_{\text{FF,SOFIA}}) = Z_{\text{FF,SOFIA}} \times N_{\text{CN}}/Z_{\text{CN}}, \qquad (2)$$

where the index CN indicates the compound nucleus. Then the predicted prompt-neutron multiplicity as a function of the atomic number of the fission fragment can be obtained from

$$\begin{aligned}\langle\nu\rangle_{\text{UCD}}(Z_{\text{FF,SOFIA}}) = {}& \langle N_{\text{FF}}^{\text{pre}}\rangle_{\text{UCD}}(Z_{\text{FF,SOFIA}}) \\ &- \langle N_{\text{FF,SOFIA}}\rangle(Z_{\text{FF,SOFIA}}), \qquad (3)\end{aligned}$$

with $\langle N_{\text{FF,SOFIA}}\rangle$, the measured number of neutrons of fission fragments, averaged over the isotopic chain per atomic number.

B. Fission as an adiabatic process in a Fermi gas

The first method to distribute the measured total prompt-neutron multiplicity between the light and heavy fission fragments is model dependent. It considers that the full excitation energy of each fission fragment translates into prompt-neutron emission at scission and that the sharing of the excitation energy between both fragments follows an adiabatic process in a Fermi gas. In this hypothesis, both nascent fission fragments, with a level density described by the Bethe formula [30], are produced with an equal temperature. As a consequence, the ratio of the masses of the primary fission fragments is equal to the ratio of the excitation energies:

$$\frac{\langle A_{\text{L}}^{\text{pre}}\rangle}{\langle A_{\text{H}}^{\text{pre}}\rangle} = \frac{\langle E_{\text{L}}^*\rangle}{\langle E_{\text{H}}^*\rangle} \sim \frac{\langle\nu_{\text{L}}\rangle}{\langle\nu_{\text{H}}\rangle}, \qquad (4)$$

$$\langle\nu_{\text{L,H}}\rangle = \langle\nu_{\text{tot,FF}}\rangle(Z_{\text{L}}, Z_{\text{H}})\frac{\langle A_{\text{L,H}}\rangle}{\langle A_{\text{L}}\rangle + \langle A_{\text{H}}\rangle}, \qquad (5)$$

where each average value is measured for each fission-fragment atomic number and where $\langle\nu_{\text{tot,FF}}\rangle$ is the total prompt-neutron multiplicity emitted by both fission partners only, as previously defined in Sec. VI. Such an approach introduces several biases which should be discussed. First, the adiabatic hypothesis differs from other descriptions such as the complete energy sorting proposed in Ref. [26]. Second, part of the excitation energy is dissipated after scission by γ emission. The latter is, however, not taken into account in

this approach. Third, this approach considers that the nascent fission fragments already gain their total and final excitation energy at scission. In fact, each fission fragment acquires some excitation energy after scission, from the relaxation of the deformation energy of the nascent fragments. Note that $\langle\nu_{\text{tot}}\rangle$ is measured for each $(Z_{\text{L}}, Z_{\text{H}})$ configuration which partly compensates the above-mentioned biases. Indeed, as illustrated in Fig. 14 for the particular case of the deformation, $\langle\nu_{\text{tot}}\rangle$ contains the information of the *sum effect* of the deformation of both fragments. Therefore, the sharing proposed in Eqs. (4) and (5) only neglects the *differential effect* between the light and heavy fragments of deformation and γ emission. Finally, the remaining bias of the approach cannot be corrected but is evaluated in Sec. VII D, based on the experimental approach introduced in Sec. VII C.

C. Combination of results from SOFIA and previous experiments

The second method to distribute the measured total prompt-neutron multiplicity between the light and heavy fission fragments relies on the experimental results from Refs. [28,31,32]. These experimental studies observed that starting from a known $\nu(A)$ distribution at low excitation energy of the fissioning system, any increase of the excitation energy translates into additional neutron emission in the heavy fission fragment only. This property, highlighted in the lower and left panel of Fig. 19 for the neutron-induced fission of ^{237}Np at two different energies [28], is used here.

Starting from the measured prompt-neutron multiplicity in neutron-induced fission at lower excitation energies, ^{237}Np(n,f) [28] and ^{233}U(n$_{\text{th}}$,f) [29], the additional prompt-neutron emission measured in Coulomb-induced fission is considered to be evaporated by the heavy fragment only. The procedure follows these steps. References [28,29] show the prompt-neutron multiplicity as a function of the mass of the primary fission fragments. First, these results are converted as a function of the atomic number of the fission fragments. This is done using the GEF model [25], by calculating the average $\langle Z\rangle$ value per mass number of the primary fission fragments for each experimental neutron beam energy. The results are presented with open green triangles in the upper left and right panels of Fig. 19 for ^{237}Np(n,f) and ^{233}U(n$_{\text{th}}$,f), respectively. Second, $\langle\nu_{\text{L}}\rangle$, the prompt-neutron multiplicity of the light fission fragment, is deduced from data at lower excitation energies. And finally, $\langle\nu_{\text{H}}\rangle$, the prompt-neutron multiplicity of the heavy fission fragment, is simply obtained by subtracting $\langle\nu_{\text{L}}\rangle$ from $\langle\nu_{\text{tot,FF}}\rangle$, the total prompt-neutron multiplicity emitted by the fission fragments only.

The prompt-neutron multiplicity as a function of the atomic number of the fission fragment, for Coulomb-induced fission, is represented by full squares and dashed lines in the lower panels of Fig. 19. The results are considered as our reference measurement hereafter, since they essentially depend on experimental data. Experimental data for the fissioning nucleus ^{238}Np are less accurate and only a restricted Z range, covering the asymmetric splits, can thus be used. In contrast, the ^{233}U(n$_{\text{th}}$,f) data are accurate enough over the whole fission-fragment range. The uncertainties of this
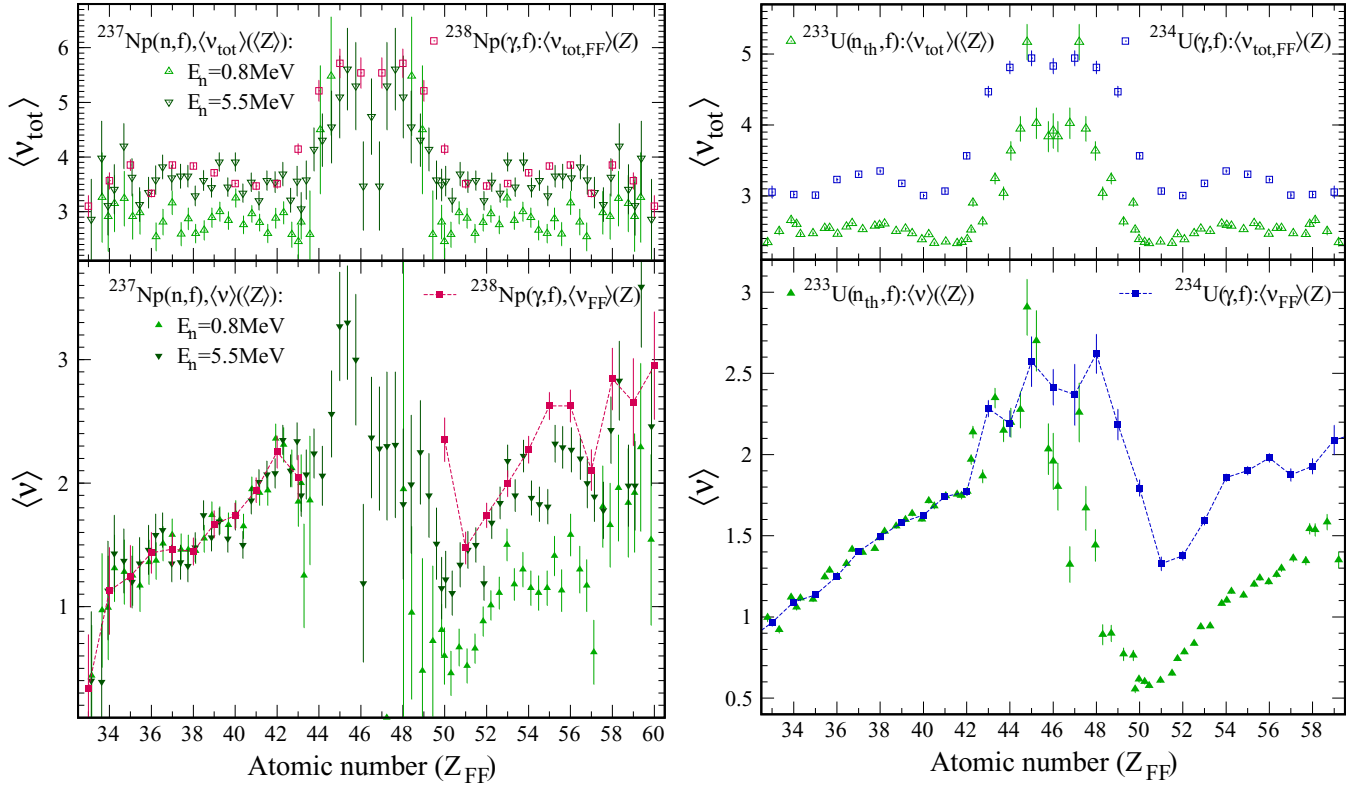
FIG. 19. Prompt-neutron multiplicity as a function of the atomic number of the fission fragment for the fissioning systems ^{238}Np (left) and ^{234}U (right). Results from ^{237}Np(n,f) [28] and ^{233}U(n$_{th}$,f) [29] are represented with green triangles as a function of Z_{FF} using GEF calculations. The average neutron multiplicity, $\langle \nu_{tot} \rangle$, measured in this work are corrected for compound nucleus emission (open squares) and distributed between both fragments (full squares) following the experimental results detailed in Refs. [28,31,32].

method have been determined taking into account the error bars of the different sets of data.

D. Prompt-neutron multiplicity as a function of the atomic number

The prompt-neutron multiplicity as a function of the atomic number of the fission fragment is presented in Fig. 20.

Both approaches to model the sharing of excitation energy between the fission fragments, based either on experimental

data (dashed lines) or on the adiabatic assumption in a Fermi gas (full lines labeled FA), agree within 0.4 units. The maximum difference is found around the ST1 mode characterized by a quasispherical heavy fission fragment. For this fission mode where the influence of the deformation plays a major role, the FA hypothesis overestimates the prompt-neutron emission of the heavy fission fragment by 0.4 neutrons, whereas the results from the experimental approach and from GEF are almost identical. In the following, this difference of 0.4 neutrons is then considered as the maximum uncertainty

TABLE VII. Prompt-neutron multiplicity for ^{234,235}U and ^{238}Np reactions, from the light and heavy fission fragments calculated with the GEF model [25], or inferred from experiment with either the adiabatic hypothesis in a Fermi gas, or the experimental-based approach, or the UCD assumption.

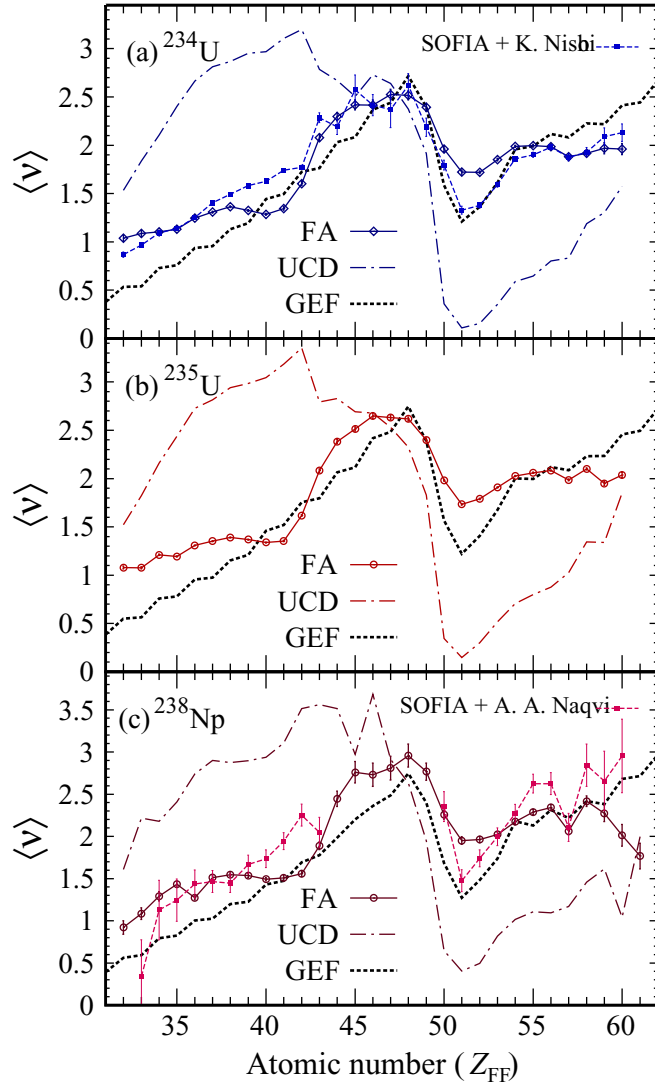|	^{234}U	^{235}U	^{238}Np
$\langle \nu_L \rangle_{GEF}$	1.0	1.0	1.2
$\langle \nu_H \rangle_{GEF}$	2.0	2.0	2.1
$\langle \nu_{tot,FF,SOFIA}^{asym} \rangle$	3.2 ± 0.1	3.3 ± 0.1	3.7 ± 0.1
$\langle \nu_L \rangle_{FA}$	$1.3 \pm 0.1 \pm 0.4$	$1.3 \pm 0.1 \pm 0.4$	$1.5 \pm 0.1 \pm 0.4$
$\langle \nu_H \rangle_{FA}$	$1.9 \pm 0.1 \pm 0.4$	$2.0 \pm 0.1 \pm 0.4$	$2.2 \pm 0.1 \pm 0.4$
$\langle \nu_L \rangle_{exp\text{-}based}$	1.4 ± 0.1		1.5 ± 0.2
$\langle \nu_H \rangle_{exp\text{-}based}$	1.8 ± 0.1		2.4 ± 0.2
$\langle \nu_L \rangle_{UCD}$	3.1	3.3	3.2
$\langle \nu_H \rangle_{UCD}$	0.2	0.3	0.4

FIG. 20. Prompt-neutron multiplicity as a function of the atomic number of the fission-fragment, for Coulomb-induced fission of ^{234,235}U and ^{238}Np in panels (a), (b), and (c), respectively. The dotted black lines present the GEF [25] calculations. The dot-dashed colored lines correspond to the results obtained from the UCD hypothesis. The full colored lines show the results of the adiabatic hypothesis applied to a Fermi gas. The dashed colored lines correspond to the results combining our data with neutron-induced fission data measured by Nishio *et al.* [29] and Naqvi *et al.* [28], for the fissioning nuclei ^{234}U and ^{238}Np, respectively. The error bars indicate the statistical uncertainties originating from the experimental data. For the adiabatic Fermi-gas assumption, an additional uncertainty of 0.4 neutrons should be added to account for the uncertainty of the model.

introduced by the FA assumption applied to our experimental data, which are characterized by a low prompt-neutron emission.

In contrast, the prompt-neutron multiplicity $\langle \nu_{L,H} \rangle_{UCD}$ calculated with the UCD hypothesis [Eq. (3)] disagrees with all the other methods with a maximum difference of two neutrons in the light fission fragment. In the UCD hypothesis, the

total prompt-neutron multiplicity is mainly distributed to the light fragment group to compensate for the weaker $\langle N_{FF} \rangle / Z_{FF}$ ratio compared to the $\langle N_{CN} \rangle / Z_{CN}$ ratio (see Fig. 17). This classical approach seems to introduce a significant bias when extracting fission observables, whereas the hypothesis based on an adiabatic energy sorting in a Fermi gas provides a more accurate mean value of the mean prompt-neutron multiplicity as a function of the atomic number.

Finally, the average prompt-neutron multiplicity is calculated for the light and heavy fission fragments produced for asymmetric fission only. For the FA hypothesis, the total prompt-neutron multiplicity $\langle \nu_{tot}^{asym} \rangle$ is first determined. In order to minimize the overlap with the SL mode, $\langle \nu_{tot}^{asym} \rangle$ is measured for the limited atomic number ranges, $Z_L = [33, 39]$ and $Z_H = [53, 59]$ for ^{234,235}U, and, $Z_L = [33, 40]$ and $Z_H = [53, 60]$ for ^{238}Np. Then, to infer the prompt-neutron multiplicity for the light and heavy fission fragments, $\langle \nu_{L,H} \rangle_{FA}$, Eq. (5) is simply applied to the measured $\langle \nu_{tot,FF}^{asym} \rangle$, obtained after correction of the prompt-neutron emission from the compound nucleus, and, to the measured $\langle A_{L,H} \rangle$ given in Table VI. For the experimental data-based approach, the average over the above-mentioned ranges is calculated from the prompt-neutron multiplicity inferred in Sec. VII C and weighted by the experimental elemental yields. Numerical values are given in Table VII. The FA and experimental data-based approaches give identical results within 1% and differ from the GEF calculations by less than 10%. The discrepancy mainly originates from the total prompt-neutron multiplicity, which is lower by 0.2 neutrons in the GEF calculation, as shown in Fig. 18. To complete the comparison, the UCD hypothesis [Eq. (3)] is applied to the measured $\langle Z_{L,H} \rangle$ from Table VI. This assumption gives a completely different pattern since almost no neutron emission originates from the heavy fission fragment.

E. Neutron excess at scission

The $\langle N_{FF}^{pre} \rangle / Z_{FF}$ ratio, defined as the neutron excess of the primary fission fragments prior to the neutron-evaporation stage, is governed by the shell effects in fission. However, this observable is difficult to obtain experimentally and data are scarce.

Therefore, Fig. 21 presents the $\langle N_{FF}^{pre} \rangle / Z_{FF}$ ratio obtained from all depicted approaches—the fully experimental-based (dashed lines and full squares, Sec. VII C), the adiabatic process in a Fermi gas (full lines and open symbols, Sec. VII B), and the UCD (dash-dotted lines, Sec. VII A)—taking our experimental results as input, in comparison with GEF calculations (dotted lines). The conclusions stated for the prompt-neutron multiplicity hold for the $\langle N_{FF}^{pre} \rangle / Z_{FF}$ ratio. All methods (except the UCD) applied to calculate the neutron excess prior to the neutron evaporation phase agree very well. The UCD hypothesis is inappropriate by definition to describe any charge polarization arising from the joint influence of proton and neutron shells. Comparison between Figs. 17 and 21 shows that the evolution of the neutron excess at scission is similar to the one after the prompt-neutron evaporation phase in our Coulomb-induced fission data, due to the low prompt-neutron emission from the fission fragments.
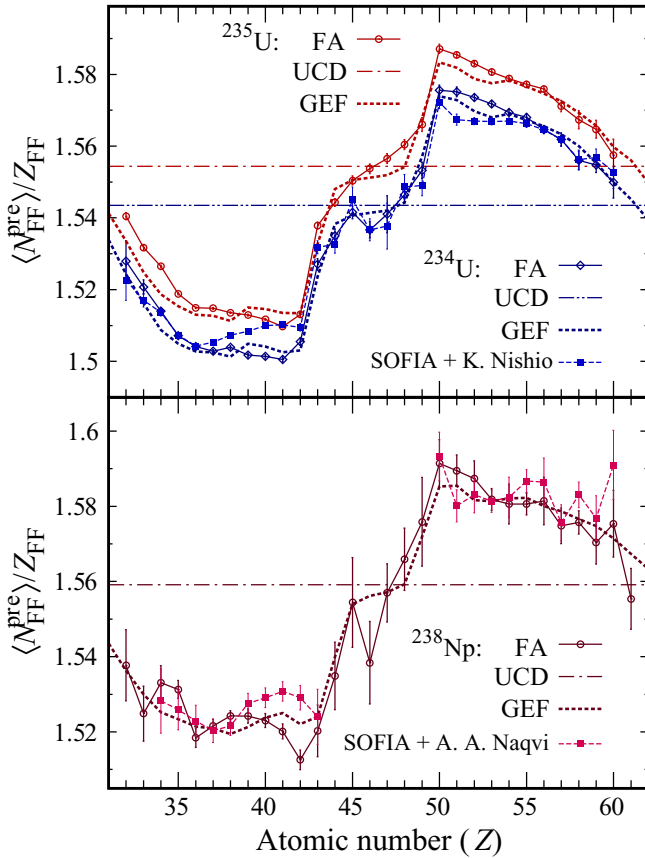
FIG. 21. Neutron excess of pre-neutron-evaporation fission fragments produced for Coulomb-induced fission, calculated from the GEF model (dotted lines [25]) and inferred based on the UCD hypothesis (horizontal lines), the experimental-based method combining our data with the measurements of Nishio [29] and Naqvi [28] for ^{234}U and ^{238}Np, respectively (dashed lines) and the adiabatic hypothesis in a Fermi gas (full lines). For the latter, an additional uncertainty of 0.4 neutrons should be added to $\langle N_{FF}^{pre}\rangle$.

F. Mean values of the number of neutrons of the primary fission fragments in asymmetric fission

In the following, we deduce the $\langle N_{L,H}^{pre}\rangle$ average values for asymmetric scission only and study their evolution as a function of the charge and mass numbers of the compound nuclei. Using the $\langle \nu_{L,H}\rangle$ values from Table VII and the measured $\langle N_{L,H}\rangle$ values from Table VI, the mean number of neutrons, $\langle N_{L,H}^{pre}\rangle$ of the primary light and heavy fission fragments are inferred. All calculations but the UCD agree very well, as shown in Table VIII. The GEF results are obtained from the calculated primary isotonic yield distributions, fitted with a sum of three Gaussian distributions.

Interestingly, despite the fact that the predictions based on the UCD approach differ by up to two neutrons, the latter nevertheless has a similar relative evolution for the various compound nuclei. Thus, the comparison of the three approaches indicates that fission of the compound nuclei in this region is characterized, as previously studied [4], with the heavy fission fragment stabilized by $Z_H = 54$, and the number of neutrons increasing with the number of neutrons of the compound nuclei. However, we extract a value of $N_H^{pre} = 85$–85.5, which is significantly different from the results of Eq. (2) and discussed in Ref. [4]. Between the fission of ^{234}U ($N_{CN} = 142$) and ^{238}Np ($N_{CN} = 145$), the number of neutrons increases much more for the light fission fragments. It reflects the population of the light group with a large difference in atomic number.

VIII. CONCLUSIONS

Elemental, isobaric, isotonic, and isotopic yields have been measured for Coulomb-induced fission of the nuclides ^{234,235}U and ^{237,238}Np. The full fission-fragment range could be investigated, using the R3B/SOFIA setup at the GSI/FRS facility. Results are obtained with an unprecedented accuracy for the ^{235}U compound nucleus, thanks to the accumulated statistics of more than 10^6 Coulomb-induced fission events. For the first time, isotopic yields are measured for the compound nuclei ^{237,238}Np. Moreover, the total prompt-neutron multiplicity is also obtained in this experiment, on an event-by-event basis, for Coulomb-induced fission of ^{234,235}U and ^{238}Np. The mean value of this multiplicity as a function of the atomic number of the fission fragments unveils the signature of fission modes: The symmetric SL fission mode is characterized by a scission configuration exhibiting very elongated nascent fragments. The total prompt-neutron multipicity is also obtained for each nuclide produced as fission fragment.

TABLE VIII. For Coulomb-induced fission of ^{234,235}U and ^{238}Np, the mean values of the measured proton numbers of Table VI are given with the neutron numbers of the primary fission fragments, inferred using all previously depicted approaches.

	^{234}U	^{235}U	^{238}Np
$\langle Z_L\rangle_{exp}$	38.1 ± 0.1	38.2 ± 0.1	39.3 ± 0.1
$\langle N_L^{pre}\rangle_{exp\text{-}based}$	57.1 ± 0.1		59.6 ± 0.2
$\langle N_L^{pre}\rangle_{FA}$	$57.0 \pm 0.1 \pm 0.4$	$57.4 \pm 0.1 \pm 0.4$	$59.6 \pm 0.2 \pm 0.4$
$\langle N_L^{pre}\rangle_{UCD}$	58.8	59.4	61.3
$\langle N_L^{pre}\rangle_{GEF}$	57.2	57.7	60.0
$\langle Z_H\rangle_{exp}$	53.9 ± 0.1	53.8 ± 0.1	53.7 ± 0.1
$\langle N_H^{pre}\rangle_{exp\text{-}based}$	84.8 ± 0.1		85.7 ± 0.2
$\langle N_H^{pre}\rangle_{FA}$	$84.9 \pm 0.1 \pm 0.4$	$85.3 \pm 0.1 \pm 0.4$	$85.5 \pm 0.2 \pm 0.4$
$\langle N_H^{pre}\rangle_{UCD}$	83.2	83.6	83.7
$\langle N_H^{pre}\rangle_{GEF}$	84.6	84.9	84.8

This offers new insight into the impact of the fission modes on the prompt-neutron emission. Notably, the multiplicity decreases as the number of the neutrons of the fragments increases, except for the element molybdenum. These particular isotopes are produced by the ST1 fission mode, but also on the neutron-rich side by the SL mode, which causes an increase of the multiplicity canceling the decrease due to the asymmetric scission mode.

Previously published data for the Coulomb-induced fission of ^{238}U(γ,f) [6], also studied with the R3B/SOFIA setup, are included in this article to illustrate the evolution of the yields along the uranium chain. The evolution of elemental yields and proton even-odd staggering shows that the increased number of neutrons in the compound nucleus leads to a higher contribution of the ST1 fission mode. This indicates a larger influence of the doubly magic ^{132}Sn nucleus, as the mass-over-charge value of the compound nucleus approaches that of ^{132}Sn.

Data from this work and from Ref. [6] for the compound nuclei ^{234,238}U are compared with data at lower excitation energy, respectively, with thermal-neutron induced fission of ^{233}U [14,20] and with fission induced after inelastic scattering of a ^{238}U beam on a ^{12}C target [15,17]. The increase in excitation energy enhances contributions from the symmetric SL mode, compared to the asymmetric modes, and decreases the global proton even-odd staggering. The local even-odd staggering is measured in this experiment with a very good precision, and the comparison along the uranium chain or with data at lower excitation energy probe the underlying influence of the proton shells. The variation of the local even-odd staggering indicates that three proton shells play a role in the asymmetric fission: $Z = 50$, $Z = 52$, and $Z = 56$. Finally, with increasing excitation energy, the global even-odd effect decreases. However, with much caution, one can observe that the extra enhancement at $Z = 52$ and $Z = 56$, the two proton shells which are predicted to be at the origin of the ST2 mode [5], does not seem to be affected by the increased excitation energy. Such an observation is in agreement with a constant shape of the potential as a function of the excitation energy.

In Ref. [4], it was observed that the Z value of the heavy fragments provides an enhanced stability. With the R3B/SOFIA experiment, this conclusion has been extended to the ^{237,238}Np fissioning nuclei. Moreover, the experimental setup used in Ref. [4] does not allow for a direct determination of the neutron number of the fission fragments. Therefore, the statement that the N value of the heavy fragments plays no role in their stabilization, was based on the UCD hypothesis, which is shown here to be not fully valid.

In this article, the same analysis with the UCD hypothesis is reproduced. The latter is usually applied when only one single observable, the mass or atomic number, is experimentally obtained. However, an alternative approach to UCD is also proposed, where the coincidence measurement of $(Z_\mathrm{L}, A_\mathrm{L})$, $(Z_\mathrm{H}, A_\mathrm{H})$, and ν_tot is used. The measured total prompt-neutron multiplicity is distributed between both fission fragments in a first step, either following the widely used adiabatic hypothesis in a Fermi gas or by combining our experimental results with the ones of other experiments measuring the prompt-neutron multiplicity per fission fragment. Then, in a second step $\langle N^\mathrm{pre} \rangle$ can be inferred at scission after neutron emission. The comparison of all methods together with results from the GEF calculations show that UCD does not manage to predict accurately absolute values for the fission observables at scission. This is understood as being due to the UCD hypothesis, which by definition washes out some effect of the nuclear structure of the fission fragments. In contrast, the deviation of the approach considering fission as an adiabatic process in a Fermi gas, with respect to the results obtained with experimental data, caused by the excitation energy sharing assumption and the fact that the deformation energy is neglected, is observed to be less than 0.4 neutrons. This small effect is valid only for Coulomb-induced fission, mainly because the value of the total prompt-neutron multiplicity is low. Indeed, when more excitation energy is transferred to the compound system, the total prompt-neutron multiplicity increases as the absolute value of the uncertainty. Moreover, with increasing excitation energy, fission of higher chances are favored and the mixing of the different fissioning systems makes interpretation more difficult. Therefore, Coulomb-induced fission is a favorable case to apply such an approach, also due to the high probability of first chance fission.

Finally, this study seems to indicate that indeed the heavy fission fragments are only stabilized around $Z_\mathrm{H} = 54$ and the associated number of neutrons vary with the number of neutrons in the compound nuclei, but with an absolute value around $N_\mathrm{H}^\mathrm{pre} = 85$ to 85.5 for the studied fissioning systems.

ACKNOWLEDGMENTS

[1] U. Brosa, Phys. Rev. C **38**, 1944 (1988).

[2] F.-J. Hambsch, H.-H. Knitter, and C. Budtz-Jørgensen, Nucl. Phys. A **491**, 56 (1989).

[3] U. Brosa, S. Grossmann, and A. Müller, Phys. Rep. **197**, 167 (1990).

[4] K.-H. Schmidt, S. Steinhäuser, C. Böckstiegel, A. Grewe, A. Heinz, A. R. Junghan, J. Benlliure, H.-G. Clerc, M. de Jong, J. Müller, M. Pfützner, and B. Voss, Nucl. Phys. A **665**, 221 (2000).

[5] G. Scamps and C. Simenel, Nature (London) **564**, 382 (2018).

[6] E. Pellereau, J. Taïeb, A. Chatillon, H. Alvarez-Pol, L. Audouin, Y. Ayyad, G. Bélier, J. Benlliure, G. Boutoux, M. Caamaño *et al.*, Phys. Rev. C **95**, 054603 (2017).

[7] A. Chatillon, J. Taïeb, H. Alvarez-Pol, L. Audouin, Y. Ayyad, G. Bélier, J. Benlliure, G. Boutoux, M. Caamaño, E. Casarejos *et al.*, Phys. Rev. C **99**, 054628 (2019).

[8] W. B. Christie, J. L. Romero, F. P. Brady, C. E. Tull, C. M. Castenada, E. F. Barasch, M. L. Webb, J. R. Drummond, H. J. Crawford, I. Flores, D. E. Greiner, P. J. Lindstrom, H. Sann, and J. C. Young, Nucl. Instrum. Methods Phys. Res., Sec. A **255**, 466 (1987).

[9] H. Geissel, P. Armbruster, K. H. Behr, A. Brünle, K. Burkard, M. Chen, H. Folger, B. Franczak, H. Keller, O. Klepper *et al.*, Nucl. Instrum. Methods Phys. Res., Sec. B **70**, 286 (1992).

[10] ALADIN Collaboration, GSI Scientific Report No. 1988, GSI 89-1, 292 (GSI, Darmstadt, Germany, 1989).

[11] J. Janik, A. Prochazka, B. Sitar, P. Strmen, I. Szarka, H. Geissel, K.-H. Behr, C. Karagiannis, C. Nociforo, H. Weick, and M. Winkler, Nucl. Instrum. Methods Phys. Res., Sec. A **640**, 54 (2011).

[12] F. Carminati *et al.* (ALICE Collaboration), J. Phys. G: Nucl. Part. Phys. **30**, 1517 (2004).

[13] A. Ebran, J. Taieb, G. Belier, A. Chatillon, B. Laurent, J.-F. Martin, and E. Pellereau, Nucl. Instrum. Methods Phys. Res., Sec. A **728**, 40 (2013).

[14] U. Quade, K. Rudolph, S. Skorka, P. Armbruster, H.-G. Clerc, W. Lang, M. Mutterer, C. Schmitt, J. P. Theobald, F. Gönnenwein *et al.*, Nucl. Phys. A **487**, 1 (1988).

[15] D. Ramos, M. Caamaño, F. Farget, C. Rodríguez-Tajes, L. Audouin, J. Benlliure, E. Casarejos, E. Clement, D. Cortina, O. Delaune *et al.*, Phys. Rev. C **97**, 054612 (2018).

[16] See the Supplemental Material at http://link.aps.org/supplemental/10.1103/PhysRevC.104.044602 for all numerical values of the fission yields and total prompt-neutron multiplicities.

[17] D. Ramos, M. Caamaño, F. Farget, C. Rodríguez-Tajes, L. Audouin, J. Benlliure, E. Casarejos, E. Clement, D. Cortina, O. Delaune *et al.*, Phys. Rev. C **99**, 024615 (2019).

[18] C. Böckstiegel, S. Steinhäuser, K.-H. Schmidt, H.-G. Clerc, A. Grewe, A. Heinz, M. de Jong, A. R. Junghans, J. Müller, and B. Voss, Nucl. Phys. A **802**, 12 (2008).

[19] B. L. Tracy, J. Chaumont, R. Klapisch, J. M. Nitschke, A. M. Poskanzer, E. Roeckl, and C. Thibault, Phys. Rev. C **5**, 222 (1972).

[20] F. Martin, C. Sage, G. Kessedjian, O. Sérot, C. Amouroux, C. O. Bacri, A. Bidaud, A. Billebaud, N. Capellan, S. Chabod *et al.*, Nucl. Data Sheets **119**, 328 (2014).

[21] M. V. Ricciardi, K.-H. Schmidt, and A. Kelić-Heil, arXiv:1007.0386.

[22] K. F. Flynn, E. P. Horwitz, C. A. A. Bloomquist, R. F. Barnes, R. K. Sjoblom, P. R. Fields, and L. E. Glendenin, Phys. Rev. C **5**, 1725 (1972).

[23] J. P. Unik, J. E. Gindler, L. E. Glendenin, K. F. Flynn, A. Gorski, and R. K. Sjoblom, in *Proceedings of the third IAEA Symposium on the Physics and Chemistry of Fission, Rochester (NY), 1973*, Vol. 2 (IAEA, Vienna, 1974), p. 19.

[24] M. Caamaño, F. Farget, O. Delaune, K. H. Schmidt, C. Schmitt, L. Audouin, C.-O. Bacri, J. Benlliure, E. Casarejos, X. Derkx *et al.*, Phys. Rev. C **92**, 034606 (2015).

[25] K.-H. Schmidt, B. Jurado, C. Amouroux, and C. Schmitt, Nucl. Data Sheets **131**, 107 (2016).

[26] K.-H. Schmidt and B. Jurado, Phys. Rev. Lett. **104**, 212501 (2010).

[27] K.-H. Schmidt and B. Jurado, Phys. Rev. C **83**, 061601(R) (2011).

[28] A. A. Naqvi, F. Käppeler, F. Dickmann, and R. Müller, Phys. Rev. C **34**, 218 (1986).

[29] K. Nishio, M. Nakashima, I. Kimura and Y. Nakagome, J. Nucl. Sci. Technol. **35**, 631 (1998)

[30] H. A. Bethe, Phys. Rev. **50**, 332 (1936).

[31] R. Müller, A. A. Naqvi, F. Käppeler, and F. Dickmann, Phys. Rev. C **29**, 885 (1984).

[32] G. N. Kniajeva, L. Krupa, A. A. Bogachev, G. G. Chubarian, O. Dorvaux, I. M. Itkis, M. G. Itkis, J. Kliman, S. Khlebnikov, N. A. Kondratiev *et al.*, Nucl. Phys. A **734** (2004)